Monthly Notices of the ROYAL ASTRONOMICAL SOCIETY

MNRAS **471,** 2370–2390 (2017) doi:10.1093/mnras/stx1641
Advance Access publication 2017 June 30

The clustering of galaxies in the completed SDSS-III Baryon Oscillation Spectroscopic Survey: single-probe measurements from DR12 galaxy clustering – towards an accurate model

Chia-Hsun Chuang,[1,2]★ Marcos Pellejero-Ibanez,[1,2,3,4] Sergio Rodríguez-Torres,[1,5,6] Ashley J. Ross,[7,8] Gong-bo Zhao,[8,9] Yuting Wang,[8,9] Antonio J. Cuesta,[10] J. A. Rubiño-Martín,[3,4] Francisco Prada,[1,6,11] Shadab Alam,[12,13] Florian Beutler,[8,14] Daniel J. Eisenstein,[15] Héctor Gil-Marín,[12,13] Jan Niklas Grieb,[16,17] Shirley Ho,[14,18,19,20] Francisco-Shu Kitaura,[2,14,20] Will J. Percival,[8] Graziano Rossi,[21] Salvador Salazar-Albornoz,[16,17] Lado Samushia,[8,22,23] Ariel G. Sánchez,[17] Siddharth Satpathy,[18,19] Anže Slosar,[24] Daniel Thomas,[8] Jeremy L. Tinker,[25] Rita Tojeiro,[26] Mariana Vargas-Magaña,[27] Jose A Vazquez,[24] Joel R. Brownstein,[28] Robert C. Nichol[8] and Matthew D Olmstead[29]

Affiliations are listed at the end of the paper

Accepted 2017 June 29. Received 2017 June 28; in original form 2016 July 12

ABSTRACT

We analyse the broad-range shape of the monopole and quadrupole correlation functions of the Baryon Oscillation Spectroscopic Survey Data Release 12 (DR12) CMASS and LOWZ galaxy sample to obtain constraints on the Hubble expansion rate $H(z)$, the angular-diameter distance $D_A(z)$, the normalized growth rate $f(z)\sigma_8(z)$ and the physical matter density $\Omega_m h^2$. We adopt wide and flat priors on all model parameters in order to ensure the results are those of a 'single-probe' galaxy clustering analysis. We also marginalize over three nuisance terms that account for potential observational systematics affecting the measured monopole. However, such Monte Carlo Markov Chain analysis is computationally expensive for advanced theoretical models. We develop a new methodology to speed up the analysis. Using the range $40\,h^{-1}$ Mpc $< s < 180\,h^{-1}$ Mpc, we obtain $\{D_A(z)r_{s,fid}/r_s$ (Mpc), $H(z)r_s/r_{s,fid}$ km s^{-1} Mpc^{-1}, $f(z)\sigma_8(z)$, $\Omega_m h^2\} = \{956 \pm 28, 75.0 \pm 4.0, 0.397 \pm 0.073, 0.143 \pm 0.017\}$ at $z = 0.32$ and $\{1421 \pm 23, 96.7 \pm 2.7, 0.497 \pm 0.058, 0.137 \pm 0.015\}$ at $z = 0.59$ where r_s is the comoving sound horizon at the drag epoch and $r_{s,fid} = 147.66$ Mpc for the fiducial cosmology used in this study. Combining our measurements with *Planck* data, we obtain $\Omega_m = 0.306 \pm 0.009$, $H_0 = 67.9 \pm 0.7$ km s^{-1} Mpc^{-1} and $\sigma_8 = 0.815 \pm 0.009$ assuming Λcold dark matter (CDM); $\Omega_k = 0.000 \pm 0.003$ and $w = -1.02 \pm 0.08$ assuming owCDM. Our results show no tension with the flat ΛCDM cosmological paradigm. This paper is part of a set that analyses the final galaxy clustering data set from Baryon Oscillation Spectroscopic Survey.

Key words: cosmological parameters – distance scale – large-scale structure of Universe – cosmology: observations.

1 INTRODUCTION

The cosmic large-scale structure from galaxy redshift surveys (GRSs) provides a powerful probe of the properties of dark energy and the time dependence of any cosmological model in a manner that is highly complementary to measurements of the cosmic microwave background (CMB) (e.g. Bennett et al. 2013; Ade et al. 2014a), supernovae (SNe) (Riess et al. 1998; Perlmutter et al. 1999) and weak lensing (see e.g. Van Waerbeke & Mellier 2003 for a review).

The number of GRSs has dramatically increased in the past decades. The 2dF Galaxy Redshift Survey (2dFGRS) (Colless et al. 2001, 2003), the Sloan Digital Sky Survey (SDSS; York et al. 2000; Abazajian et al. 2009), the WiggleZ (Drinkwater

★ E-mail: chiahsun.chuang@gmail.com

et al. 2010; Parkinson et al. 2012) have collected hundreds of thousands of galaxy redshifts. The Baryon Oscillation Spectroscopic Survey (BOSS; Dawson et al. 2013) of the SDSS-III (Eisenstein et al. 2011) has observed 1.5 million luminous red galaxies (LRGs) at $0.1 < z < 0.7$ over 10 000 deg^2. The newest BOSS data set has been made publicly available in SDSS Data Release 12 (DR12; Alam et al. 2015b). The planned space mission *Euclid*[1] will survey over 30 million emission-line galaxies at $0.7 < z < 2$ over 15 000 deg^2 (e.g. Laureijs et al. 2011), and the upcoming ground-based experiment DESI[2] (Dark Energy Spectroscopic Instrument) will survey 20 million galaxy redshifts up to $z = 1.7$ and 600 000 quasars ($2.2 < z < 3.5$) over 14 000 deg^2 (Schlegel et al. 2011). The proposed *WFIRST*[3] satellite would map 17 million galaxies in the redshift range $1.3 < z < 2.7$ over 3400 deg^2, with a larger area possible with an extended mission (Green et al. 2012).

The methodologies of the data analyses of galaxy clustering have also developed along with the growing survey volumes. The observed galaxy data have been analysed, and the cosmological results delivered (see e.g. Chuang et al. 2016 for more references). In principle, the Hubble expansion rate $H(z)$, the angular-diameter distance $D_A(z)$, the normalized growth rate $f(z)\sigma_8(z)$, and the physical matter density $\Omega_m h^2$ can be well constrained by analysing the galaxy clustering data alone. Eisenstein et al. (2005) demonstrated the feasibility of measuring $\Omega_m h^2$ and an effective distance, $D_V(z)$, from the SDSS DR3 (Abazajian et al. 2005) LRGs, where $D_V(z)$ corresponds to a combination of $H(z)$ and $D_A(z)$. Chuang & Wang (2012) measured $H(z)$ and $D_A(z)$ simultaneously using the galaxy clustering data from the two-dimensional two-point correlation function of SDSS DR7 (Abazajian et al. 2009) LRGs. The methodology has been commonly known as the application of Alcock–Paczynski effect (Alcock & Paczynski 1979) on a large-scale structure. The methodology has been improved and also applied to different galaxy samples [see e.g. Blake et al. 2012; Reid et al. 2012; Chuang & Wang 2013a,b; Xu et al. 2013].

Galaxy clustering allows us to differentiate between smooth dark energy and modified gravity as the cause for cosmic acceleration through the simultaneous measurements of the cosmic expansion history $H(z)$ and the growth rate of cosmic large-scale structure, $f(z)$ (Guzzo et al. 2008; Wang 2008; Blake et al. 2012). However, measuring $f(z)$ requires measuring higher-order statistics of the galaxy clustering (see Verde et al. 2002). Song & Percival (2009) proposed using the normalized growth rate, $f(z)\sigma_8(z)$, which summarizes the growth rate measured from the two-point clustering statistics. Percival & White (2009) developed a method to measure $f(z)\sigma_8(z)$ and applied it on simulations. Wang (2012) estimated expected statistical constraints on dark energy and modified gravity, including redshift-space distortions and other constraints from galaxy clustering, using a Fisher matrix formalism. One can measure $f(z)\sigma_8(z)$ from observed data in addition to $H(z)$ and $D_A(z)$ (e.g. see Blake et al. 2012; Reid et al. 2012; Samushia, Percival & Raccanelli 2012; Chuang et al. 2013; Anderson et al. 2014a; Beutler et al. 2014; Samushia et al. 2014; Wang 2014; Chuang et al. 2016) determined $f(z)\sigma_8(z)$ from the SDSS DR7 LRGs. Blake et al. (2012) measured $H(z)$, $D_A(z)$ and $f(z)\sigma_8(z)$ from the WiggleZ Dark Energy Survey galaxy sample. Analyses have been performed to measure $H(z)$, $D_A(z)$ and $f(z)\sigma_8(z)$ from the SDSS BOSS galaxy sample (Reid et al. 2012; Chuang et al. 2013, 2016; Anderson et al. 2014a; Beutler et al. 2014; Samushia et al. 2014; Wang 2014; Alam et al. 2015a; Gil-Marín et al. 2016b).

We aim to measure $H(z)$, $D_A(z)$ and $f(z)\sigma_8(z)$ based on the observed anisotropic galaxy clustering measurement from the final BOSS data release, along the same lines, as a series of companion papers (Gil-Marín et al. 2016b; Beutler et al. 2017a; Grieb et al. 2017; Satpathy et al. 2017; Sanchez et al. 2017b). However, these complementary works either adopt the best-fitting values for $\Omega_c h^2$, $\Omega_b h^2$ and n_s (Gil-Marín et al. 2016b; Beutler et al. 2017a; Grieb et al. 2017; Sanchez et al. 2017b) or the 1σ Gaussian priors (Satpathy et al. 2017) from the *Planck* measurements to construct their theoretical models. In this work, we relax these assumptions using wide priors following Chuang et al. (2016). In particular, we allow for 10σ deviations, to minimize the potential bias from priors, so that one can safely combine our single-probe measurements with other data sets (i.e. CMB, SNe, etc.) to constrain the cosmological parameters of a given dark energy model. Meanwhile, we also include a model to minimize the impact from the observational systematics as done in Chuang et al. (2016). However, due to the large parameter space, the Monte Carlo Markov Chain (MCMC) analysis becomes expensive and that makes it difficult to use complex models, which are computationally slow, and thus we will call these complex models slow models. One would need to use very strong priors, e.g. fixing values or 1σ Gaussian priors, when extracting cosmological constraints.

To cope with this challenge, we develop in this study a new methodology to speed up the analysis when using a slow model. This includes two steps: (1) generation of Markov chains with a computationally fast model (less accurate), which we will refer to from here on as fast model; (2) replacement/calibration of the likelihoods with an accurate model (slow). For convenience, we use the 'Gaussian streaming model' described in Reid & White (2011), while we should mention that there have been more developments, e.g. Carlson, Reid & White (2013), Wang, Reid & White (2014), Taruya, Nishimichi & Bernardeau (2013), Vlah et al. (2013), White (2014), Taruya et al. (2014), Bianchi, Chiesa & Guzzo (2015), Vlah, White & Aviles (2015), Okumura et al. (2015). Although the model we use might not be the most accurate model to date, it is good enough for our purposes and the scale ranges used in this study, as we will demonstrate below. In addition, in Pellejero-Ibanez et al. (2017) (one of our companion papers), we develop and demonstrate the methodology to summarize a joint data set of galaxy sample and CMB data without introducing informative priors.

This paper is organized as follows. In Section 2, we introduce the SDSS-III/BOSS DR12 galaxy sample and mock catalogues used in our study. In Section 3, we describe the details of the methodology that constrains cosmological parameters from our galaxy clustering analysis. In Section 4, we present our single-probe cosmological measurements. In Section 5, given some simple dark energy models, we present the cosmological constraints from our measurements and the combination with other data sets. We compare our results with other studies in Section 6. We summarize and conclude in Section 7.

2 DATA SETS

2.1 The CMASS and LOWZ galaxy catalogues

The SDSS (Fukugita et al. 1996; Gunn et al. 1998; York et al. 2000; Smee et al. 2013) mapped over one quarter of the sky using the dedicated 2.5 m Sloan Telescope (Gunn et al. 2006). The Baryon Oscillation Sky Survey (BOSS; Eisenstein et al. 2011; Bolton et al. 2012; Dawson et al. 2013) is part of the SDSS-III survey. It has collected

[1] http://sci.esa.int/euclid
[2] http://desi.lbl.gov/
[3] http://wfirst.gsfc.nasa.gov/

the spectra and redshifts for 1.5 million galaxies, 160 000 quasars and 100 000 ancillary targets. The DR 12 (Alam et al. 2015b) has been made publicly available.[4] We use galaxies from the SDSS-III BOSS DR12 CMASS catalogue in the redshift range $0.43 < z < 0.75$ and LOWZ catalogue in the range $0.15 < z < 0.43$. CMASS samples are selected with an approximately constant stellar mass threshold (Eisenstein et al. 2011) and LOWZ sample consists of red galaxies at $z < 0.4$ from the SDSS DR8 (Aihara et al. 2011) image data. We are using 800 853 CMASS galaxies and 361 775 LOWZ galaxies. Note that the number of galaxies used in this study is slightly smaller than the one used by the Alam et al. (2017) (BOSS collaboration paper for final data release) by ∼40 000. The difference is in the LOWZ sample used (see Alam et al. 2017 for details). The effective redshifts of these sample are $z = 0.59$ and $z = 0.32$, respectively. The details of generating these samples are described in Reid et al. (2016). In addition, we split both CMASS and LOWZ samples into two redshift bins (four bins in total). The effective redshifts are $\{0.24, 0.37, 0.49, 0.64\}$; and numbers of galaxies are $\{154367, 207408, 425612, 375241\}$.

2.2 Mock catalogues

In this study we rely on a set of 2000 mock galaxy catalogues explicitly produced to resemble the clustering of the BOSS DR12 data. In particular we make use of the MD-PATCHY BOSS DR12 mock galaxy catalogues (Kitaura et al. 2016b). These mocks are generated with the PATCHY code (Kitaura, Yepes & Prada 2014; Kitaura et al. 2015). The calibration was performed on accurate N-body-based reference catalogues using halo abundance matching to reproduce the number density, clustering bias, selection function and survey geometry of the BOSS data on 10 redshift bins (Rodríguez-Torres et al. 2016). The mock catalogues were constructed assuming ΛCDM *Planck* cosmology with $\{\Omega_{\rm M} = 0.307115,\ \Omega_{\rm b} = 0.048206,\ \sigma_8 = 0.8288,\ n_{\rm s} = 0.96\}$, and a Hubble constant ($H_0 = 100\,h\,{\rm km\,s^{-1}\,Mpc^{-1}}$) given by $h = 0.6777$. As shown in a mock catalogue comparison study (Chuang et al. 2015), PATCHY mocks are accurate within 5 per cent on scales larger than 5 Mpc h^{-1} (or k smaller than 0.5 h Mpc^{-1} in Fourier space) for monopole and within 10–15 per cent for quadrupole. Kitaura et al. (2016b) had also demonstrated the accuracy of BOSS PATCHY mock catalogues which are in very good agreement with the observed data in terms of two- and three-point statistics. These mocks have been used in recent galaxy clustering studies (Cuesta et al. 2016; Gil-Marín et al. 2016a,b; Rodríguez-Torres et al. 2016; Slepian et al. 2017a) and void clustering studies (Kitaura et al. 2016a; Liang et al. 2016). They are also used in Alam et al. (2017) (BOSS collaboration paper for final data release) and its companion papers including this paper and Slepian et al. (2016, 2017b); Vargas-Magaña et al. (2016); Beutler et al. (2017a,b); Grieb et al. (2017); Pellejero-Ibanez et al. (2017); Ross et al. (2017); Salazar-Albornoz et al. (2017); Sanchez et al. (2017a,b); Satpathy et al. (2017); Wang et al. (2017; Zhao et al. (2017)).

3 METHODOLOGY

In this section, we describe the measurement of the multipoles of the correlation function from the observational data, construction of the theoretical prediction, and the likelihood analysis that leads to constraining cosmological parameters and dark energy.

[4] http://www.sdss3.org/

3.1 Two-dimensional two-point correlation function

We convert the measured redshifts of the BOSS CMASS and LOWZ galaxies to comoving distances by assuming a fiducial model, i.e. flat ΛCDM with $\Omega_{\rm m} = 0.307115$ and $h = 0.6777$ which is the same model adopted for constructing the mock catalogues (see Kitaura et al. 2016b). We use the two-point correlation function estimator given by Landy & Szalay (1993):

$$\xi(s,\mu) = \frac{DD(s,\mu) - 2DR(s,\mu) + RR(s,\mu)}{RR(s,\mu)}, \tag{1}$$

where s is the separation of a pair of objects and μ is the cosine of the angle between the directions between the line of sight (LOS) and the line connecting the pair the objects. DD, DR and RR represent the normalized data–data, data–random and random–random pair counts, respectively, for a given distance range. The LOS is defined as the direction from the observer to the centre of a galaxy pair. Our bin size is $\Delta s = 1\,h^{-1}$ Mpc and $\Delta\mu = 0.01$. The Landy and Szalay estimator has minimal variance for a Poisson process. The random catalogue is generated with the radial and angular selection function of the observed galaxies. One can reduce the shot noise due to random data by increasing the amount of random points. The number of random data we use is about 50 times that of the observed galaxies. While calculating the pair counts, we assign to each data point a radial weight of $1/[1 + n(z) \times P_w]$, where $n(z)$ is the radial number density and $P_w = 1 \times 10^4\,h^{-3}\,{\rm Mpc}^3$ (see Feldman, Kaiser & Peacock 1994). We include the combination of the observational weights assigned for each galaxy by

$$w_{{\rm tot},i} = w_{{\rm sys},i} * (w_{rf,i} + w_{fc,i} - 1), \tag{2}$$

where $w_{{\rm tot},i}$ is the final weight to assign on a galaxy i; $w_{{\rm sys},i}$ is for removing the correlation between CMASS galaxies and both stellar density and seeing; $w_{rf,i}$ and $w_{fc,i}$ correct for missing objects due to the redshift failure and fibre collision. The details are described in Reid et al. (2016) (see also Ross et al. 2012). Later, we will also test the impact of systematics by removing $w_{{\rm sys},i}$ from the analysis.

3.2 Multipoles of the two-point correlation function

The traditional multipoles of the two-point correlation function, in redshift space, are defined by

$$\xi_l(s) \equiv \frac{2l+1}{2}\int_{-1}^{1} {\rm d}\mu\, \xi(s,\mu) P_l(\mu), \tag{3}$$

where $P_l(\mu)$ is the Legendre Polynomial (l =0 and 2 here). We integrate over a spherical shell with radius s, while actual measurements of $\xi(s,\mu)$ are done in discrete bins. To compare the measured $\xi(s,\mu)$ and our theoretical model, the last integral in equation (3) should be converted into a sum,

$$\hat{\xi}_l(s) \equiv \frac{\sum_{s-\frac{\Delta s}{2}<s'<s+\frac{\Delta s}{2}} \sum_{0\le\mu\le1} (2l+1)\xi(s',\mu)P_l(\mu)}{\text{Number of bins used in the numerator}}, \tag{4}$$

where $\Delta s = 5\,h^{-1}$ Mpc in this work.

Fig. 1 shows the monopole ($\hat{\xi}_0$) and quadrupole ($\hat{\xi}_2$) measured from the BOSS CMASS and LOWZ galaxy sample compared with the best-fitting theoretical models. We split both CMASS and LOWZ sample into two redshift bins and show the multipoles from these four bins in Fig. 2.

We are using the scale range $s = 40 - 180\,h^{-1}$ Mpc and the bin size is $5\,h^{-1}$ Mpc. Figs 1 and 2 show the measured multipoles from

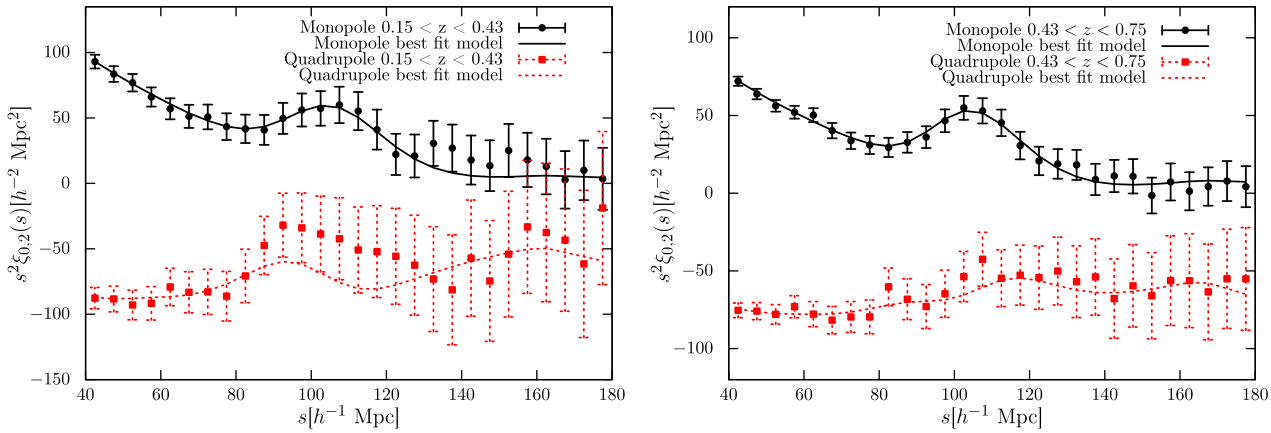

Figure 1. Measurement of monopole and quadrupole of the correlation function from two redshift bins. Left panel: measurements from the BOSS DR12 LOWZ galaxy sample within $0.15 < z < 0.43$ compared to the best-fitting theoretical models (solid lines). The χ^2 per degree of freedom (d.o.f.) is 0.91. Right panel: measurements from the BOSS DR12 CMASS galaxy sample within $0.43 < z < 0.75$ compared to the best-fitting theoretical models (solid lines). The χ^2/d.o.f. is 1.07. The error bars are the square root of the diagonal elements of the covariance matrix. In this study, our fitting scale ranges are $40\,h^{-1}$ Mpc $< s < 180\,h^{-1}$ Mpc; the bin size is $5\,h^{-1}$ Mpc.

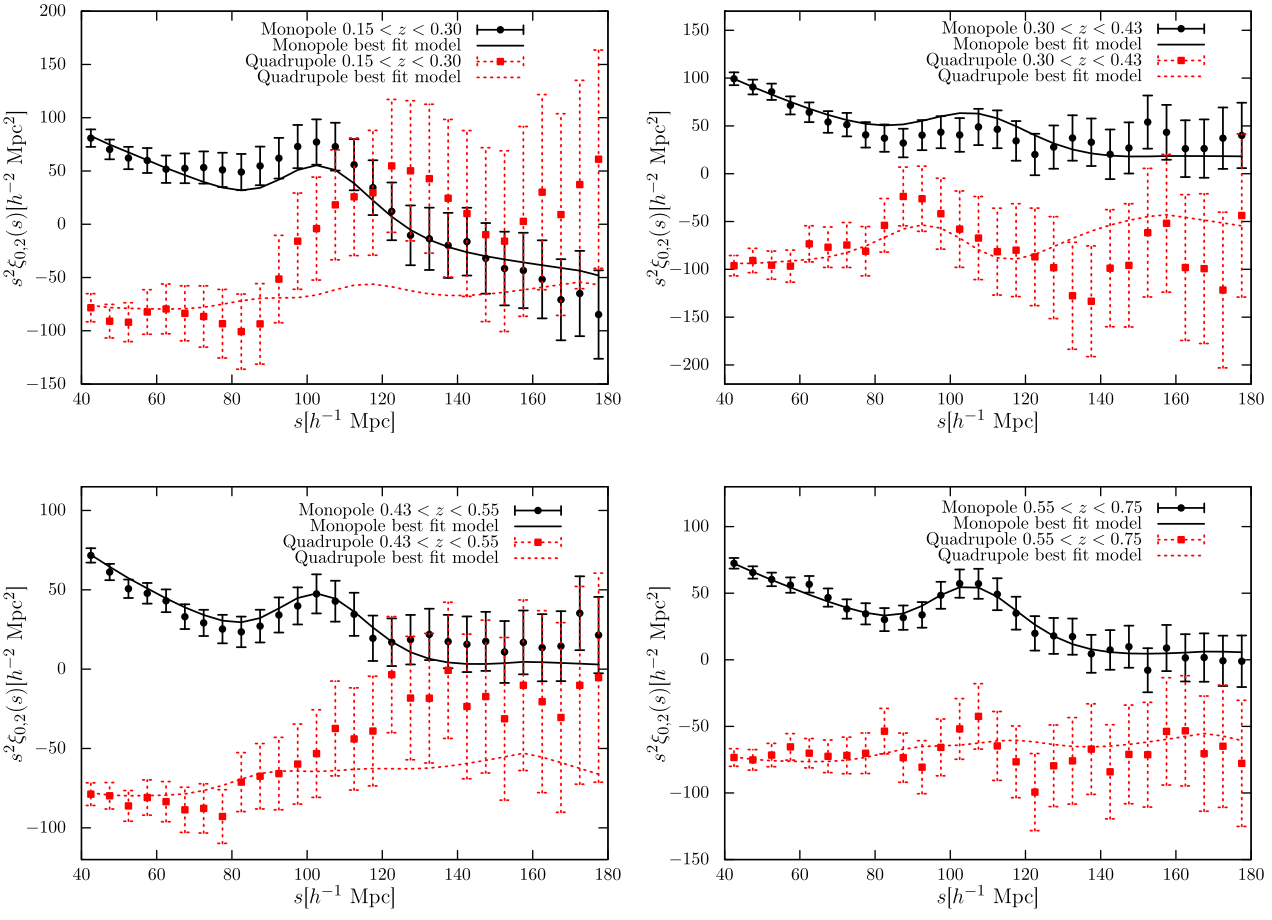

Figure 2. Measurement of monopole and quadrupole of the correlation function from four redshift bins. Top left panel: measurements from the BOSS DR12 LOWZ galaxy sample within $0.15 < z < 0.30$ compared to the best-fitting theoretical models (solid lines). The χ^2/d.o.f. is 0.71. Top right panel: measurements from the BOSS DR12 LOWZ galaxy sample within $0.30 < z < 0.43$ compared to the best-fitting theoretical models (solid lines). The χ^2/d.o.f. is 1.20. Bottom left panel: measurements from the BOSS DR12 CMASS galaxy sample within $0.43 < z < 0.55$ compared to the best-fitting theoretical models (solid lines). The χ^2/d.o.f. is 1.15. Bottom right panel: measurements from the BOSS DR12 CMASS galaxy sample within $0.55 < z < 0.75$ compared to the best-fitting theoretical models (solid lines). The χ^2/d.o.f. is 0.85. The error bars are the square root of the diagonal elements of the covariance matrix. In this study, our fitting scale ranges are $40\,h^{-1}$ Mpc $< s < 180\,h^{-1}$ Mpc; the bin size is $5\,h^{-1}$ Mpc.

various redshift ranges and their best fits. The theoretical models will be described in the next section.

3.3 Theoretical two-point correlation function

We use two theoretical models for this study. One is the two-dimensional dewiggle model (Eisenstein, Seo & White 2007) and the other is the Gaussian streaming model (Reid & White 2011). The former model is very fast but less accurate for high bias tracers; the latter is more accurate but much slower in terms of computation. We develop a new methodology to take the advantages from both of them.

3.3.1 Fast model – two-dimensional dewiggle model

We use the fast model (two-dimensional dewiggle model) which includes the linear bias, non-linear evolution at BAO scales, linear redshift-space distortion and non-linear redshift-space distortion at BAO scales on top of the linear theoretical model. The theoretical model can be constructed by first- and higher-order perturbation theory. The procedure of constructing our fast model in redshift space is the following: First, we adopt the cold dark matter (CDM) model and the simplest inflation model (adiabatic initial condition). Thus, we can compute the linear matter power spectra, $P_{\rm lin}(k)$, by using CAMB (Code for Anisotropies in the Microwave Background; Lewis, Challinor & Lasenby 2000). The linear power spectrum can be decomposed into two parts:

$$P_{\rm lin}(k) = P_{\rm nw}(k) + P^{\rm lin}_{\rm BAO}(k), \tag{5}$$

where $P_{\rm nw}(k)$ is the 'no-wiggle' or pure CDM power spectrum calculated using equation (29) from Eisenstein & Hu (1998). $P^{\rm lin}_{\rm BAO}(k)$ is the 'wiggled' part defined by equation (5). The non-linear damping effect of the 'wiggled' part, in redshift space, can be well approximated following Eisenstein et al. (2007) by

$$P^{nl}_{\rm BAO}(k,\mu_k) = P^{\rm lin}_{\rm BAO}(k)\cdot\exp\left(-\frac{k^2}{2k_\star^2}[1+\mu_k^2(2f+f^2)]\right), \tag{6}$$

where μ_k is the cosine of the angle between $\boldsymbol{k}$ and the LOS, f is the growth rate, and $k_\star$ is computed following Crocce & Scoccimarro (2006) and Matsubara (2008) by

$$k_\star = \left[\frac{1}{3\pi^2}\int P_{\rm lin}(k){\rm d}k\right]^{-1/2}. \tag{7}$$

The dewiggled power spectrum is

$$P_{\rm dw}(k,\mu_k) = P_{\rm nw}(k) + P^{nl}_{\rm BAO}(k,\mu_k). \tag{8}$$

Besides the non-linear redshift distortion introduced above, we include the linear redshift distortion as follows in order to obtain the galaxy power spectrum in redshift space at large scales (Kaiser 1987),

$$P^s_g(k,\mu_k) = b^2(1+\beta\mu_k^2)^2 P_{\rm dw}(k,\mu_k), \tag{9}$$

where b is the linear galaxy bias and $\beta = f/b$ is the linear redshift distortion parameter.

We compute the theoretical two-point correlation function, $\xi(s,\mu)$, by Fourier transforming the non-linear power spectrum $P^s_g(k,\mu_k)$. This task is efficiently performed by using Legendre polynomial expansions and one-dimensional integral convolutions as introduced in Chuang & Wang (2013a).

The purpose of using fast model is to mimic the slow model in a very efficient way. We thus define the following calibration functions to the fast model:

$$\xi_0^{cal}(s) = (1-{\rm e}^{-\frac{s}{s_1}}+{\rm e}^{-\left(\frac{s}{s_2}\right)^2})\xi_0(s), \tag{10}$$

$$\xi_2^{cal}(s) = (1-{\rm e}^{-\frac{s}{s_3}}+{\rm e}^{-\left(\frac{s}{s_4}\right)^2})\xi_2(s), \tag{11}$$

where we find the calibration parameters, $s_1 = 12$, $s_2 = 14$, $s_3 = 20$ and $s_4 = 27\,h^{-1}$ Mpc, by comparing the fast and slow models from a visual inspection. Later, we will explain that the calibration parameters will speed up the convergence but will not bias the results when doing an MCMC analysis. Therefore, it is not critical to find the optimal form of calibration function and its parameters.

3.3.2 Slow model – Gaussian streaming model

We use an advanced model called Gaussian streaming model described in Reid & White (2011). The model assumes the pairwise velocity probability distribution function is Gaussian and can be used to relate real space clustering and pairwise velocity statistics of haloes to their clustering in redshift space by

$$1+\xi^s_{\rm g}(r_\sigma, r_\pi)$$

$$= \int\left[1+\xi^r_{\rm g}(r)\right]{\rm e}^{-[r_\pi - y - \mu v_{12}(r)]^2/2\sigma^2_{12}(r,\mu)}\frac{dy}{\sqrt{2\pi\sigma^2_{12}(r,\mu)}}, \tag{12}$$

where r_σ and r_π are the redshift-space transverse and LOS distances between two objects with respect to the observer, y is the *real* space LOS pair separation, $\mu = y/r$, $\xi^{\rm r}_{\rm g}$ and $\xi^{\rm s}_{\rm g}$ are the real and redshift-space galaxy correlation functions, respectively, $v_{12}(r)$ is the average infall velocity of galaxies separated by real-space distance r, and $\sigma^2_{12}(r,\mu)$ is the rms dispersion of the pairwise velocity between two galaxies separated with transverse (LOS) real space separation r_σ (y). $\xi^{\rm r}_{\rm g}(r)$, $v_{12}(r)$ and $\sigma^2_{12}(r,\mu)$ are computed in the framework of Lagrangian ($\xi^{\rm r}$) and standard perturbation theories (v_{12}, σ^2_{12}).

For large scales, only one nuisance parameter is necessary to describe the clustering of a sample of haloes or galaxies in this model: $b_{1L} = b - 1$, the first-order Lagrangian host halo bias in *real* space. One would need another parameter, $\sigma^2_{\rm FoG}$, to model an additive, isotropic velocity dispersion accounting for small-scale motions of haloes and galaxies (one halo term). However, in this study, we consider relative large scales (i.e. $40 < s < 180\,h^{-1}$ Mpc), so that we do not include this parameter. Further details of the model, its numerical implementation and its accuracy can be found in Reid & White (2011).

3.3.3 Model for observational systematic errors

It is well known that the observations could be contaminated by systematic effects [e.g. see Ross et al. (2012) and Ross et al. (2016; companion paper)]. To obtain robust and conservative measurements, we include a model for systematics. The model is a simple polynomial given by

$$A(s) = a_0 + \frac{a_1}{s} + \frac{a_2}{s^2}, \tag{13}$$

where a_0, a_1 and a_2 are nuisance parameters. Following Chuang et al. (2016), we only include the systematics model for the monopole of the correlation function since the quadrupole is insensitive to the systematics effects of which we are aware. On the other hand, if we add another polynomial to the quadrupole as it is usually done in papers of measuring BAO only (e.g. Anderson

et al. 2014a; Cuesta et al. 2016), we would not be able to extract any information from redshift-space distortions.

3.4 Covariance matrix

We use the 2000 mock catalogues created by Kitaura et al. (2016b) for the BOSS DR12 CMASS and LOWZ galaxy sample to estimate the covariance matrix of the observed correlation function. We calculate the multipoles of the correlation functions of the mock catalogues and construct the covariance matrix as

$$\mathbf{C}_{ij} = \frac{1}{(N-1)(1-D)} \sum_{k=1}^{N} \left(\bar{\boldsymbol{X}}_i - \boldsymbol{X}_i^k\right)\left(\bar{\boldsymbol{X}}_j - \boldsymbol{X}_j^k\right), \tag{14}$$

where

$$D = \frac{N_\mathrm{b}+1}{N-1}, \tag{15}$$

N is the number of the mock catalogues, N_b is the number of data bins, $\bar{\boldsymbol{X}}_m$ is the mean of the mth element of the vector from the mock catalogue multipoles and $\boldsymbol{X}_m^k$ is the value in the mth elements of the vector from the kth mock catalogue multipoles. We are using the scale range $s = 40 - 180\,h^{-1}$ Mpc and the bin size is 5 h^{-1} Mpc. The data points from the multipoles in the scale range considered are combined to form a vector, X, i.e.

$$\boldsymbol{X} = \left\{\hat{\xi}_0^{(1)}, \hat{\xi}_0^{(2)}, ..., \hat{\xi}_0^{(N)}; \hat{\xi}_2^{(1)}, \hat{\xi}_2^{(2)}, ..., \hat{\xi}_2^{(N)}; ...\right\}, \tag{16}$$

where N is the number of data points in each measured multipole; here $N = 28$ is the same for all the redshift bins. The length of the data vector $\boldsymbol{X}$ depends on the number of multipoles used. We also include the correction, D, introduced by Hartlap, Simon & Schneider (2007).

3.5 Likelihood

The likelihood is taken to be proportional to $\exp(-\chi^2/2)$ (Press et al. 2007), with χ^2 given by

$$\chi^2 \equiv \sum_{i,j=1}^{N_X} \left[\boldsymbol{X}_{\mathrm{th},i} - \boldsymbol{X}_{\mathrm{obs},i}\right] \mathbf{C}_{ij}^{-1} \left[\boldsymbol{X}_{\mathrm{th},j} - \boldsymbol{X}_{\mathrm{obs},j}\right] \tag{17}$$

where N_X is the length of the vector used, $\boldsymbol{X}_\mathrm{th}$ is the vector from the theoretical model, and $\boldsymbol{X}_\mathrm{obs}$ is the vector from the observed data.

As explained in Chuang & Wang (2012), instead of recalculating the observed correlation function while computing for different models, we rescale the theoretical correlation function to avoid rendering the χ^2 values arbitrary (the amount of information from data sample used needs to be fixed when computing χ^2.). This approach can be considered as an application of Alcock–Paczynski effect (Alcock & Paczynski 1979). The rescaled theoretical correlation function is computed from

$$T^{-1}(\xi_\mathrm{th}(\sigma,\pi)) = \xi_\mathrm{th}\left(\frac{D_\mathrm{A}(z)}{D_\mathrm{A}^\mathrm{fid}(z)}\sigma, \frac{H^\mathrm{fid}(z)}{H(z)}\pi\right), \tag{18}$$

where ξ_th is the theoretical model described in Section 3.3, and χ^2 can be rewritten as

$$\chi^2 \equiv \sum_{i,j=1}^{N_X} \left\{\mathbf{T}^{-1}\boldsymbol{X}_{\mathrm{th},i} - \boldsymbol{X}_{\mathrm{obs},i}^\mathrm{fid}\right\} \mathbf{C}_{ij}^{-1} \cdot \left\{\mathbf{T}^{-1}\boldsymbol{X}_{\mathrm{th},j} - \boldsymbol{X}_{\mathrm{obs},j}^\mathrm{fid}\right\}; \tag{19}$$

where $\mathbf{T}^{-1}\boldsymbol{X}_\mathrm{th}$ is the vector computed from equation (4) from the rescaled theoretical correlation function (equation 18). $\boldsymbol{X}_\mathrm{obs}^\mathrm{fid}$ is the vector from observed data measured with the fiducial model (see Chuang & Wang 2012 for more details regarding the rescaling method).

3.6 Markov Chain Monte Carlo Likelihood Analysis

3.6.1 Basic procedure

We perform Markov Chain Monte Carlo likelihood analyses using COSMOMC (Lewis & Bridle 2002). The parameter space that we explore spans the parameter set of $\{H(z), D_\mathrm{A}(z), \Omega_\mathrm{m}h^2, \beta(z), b\sigma_8(z), \Omega_\mathrm{b}h^2, n_\mathrm{s}, b(z), a_0, a_1, a_2\}$. The quantities Ω_m and Ω_b are the matter and baryon density fractions, n_s is the power-law index of the primordial matter power spectrum, h is the dimensionless Hubble constant ($H_0 = 100h$ km s^{-1} Mpc^{-1}), and $\sigma_8(z)$ is the normalization of the power spectrum. The linear redshift distortion parameter can be expressed as $\beta(z) = f(z)/b$. Thus, one can derive $f(z)\sigma_8(z)$ from the measured $\beta(z)$ and $b\sigma_8(z)$. Among these parameters, only $\{H(z), D_\mathrm{A}(z), \Omega_\mathrm{m}h^2, \beta(z), b\sigma_8(z)\}$ are well constrained using the BOSS galaxy sample alone in the scale range of interest. We marginalize over the other six parameters, $\{\Omega_\mathrm{b}h^2, n_\mathrm{s}, b, a_0, a_1, a_2\}$, assuming a flat prior over the range $\{(0.01877, 0.02537), (0.8676, 1.0556), (1.5, 2.5), (-0.003, 0.003), (-3, 3), (-20, 20)\}$ respectively, where the flat priors on $\Omega_\mathrm{b}h^2$ and n_s are centred on the Planck measurements with a width of $\pm 10\sigma_{Planck}$ (σ_{Planck} is taken from Ade et al. 2014b). These priors are sufficiently wide to ensure that CMB constraints are not double counted when our results are combined with CMB data (Chuang, Wang & Hemantha 2012).

3.6.2 Generate/calibrate Markov chains with fast/slow model

We first use the fast model (2D dewiggle model) to compute the likelihood, $\mathcal{L}_\mathrm{fast}$ and generate the Markov chains. This step will make many trials (keep or throw away based on the MCMC algorithm) and eventually provides the chains of parameter points describing the parameter constraints and exclude the low likelihood regions of the parameter space.

Once we have the chains generated using the fast model, we modify the weight of each point in the chains by

$$\mathcal{W}_\mathrm{new} = \mathcal{W}_\mathrm{old}\frac{\mathcal{L}_\mathrm{slow}}{\mathcal{L}_\mathrm{fast}}, \tag{20}$$

where $\mathcal{L}_\mathrm{slow}$ and $\mathcal{L}_\mathrm{fast}$ are the likelihoods for a given point of input parameters in the chains and $\mathcal{W}_\mathrm{old}$ is the original weight of the given point. We save time by computing only the 'important' points without computing the likelihood of a point which we will not include eventually. The methodology is known as 'importance sampling'. However, the typical application of the importance sampling method is to add a likelihood from some additional data set to a given set of chains, but in this study, we will use it to replace the likelihood of a data set with a more accurate version.

It takes about 9 h to find the best-fitting value using CosmoMC (i.e. action=2) with the slow model and 30 min (18 times faster) with the fast model. The whole importance sampling (including both steps of using fast and slow models) to have the R-1 convergence value (variance of chain means/mean of chain variances) lower than 0.1 takes about 50 h using one Intel node (16 cores) of TeideHPC supercomputer.

On the scales we use for comparison with the BOSS galaxy data, the theoretical correlation function only depends on cosmic curvature and dark energy through the parameters $H(z)$, $D_\mathrm{A}(z)$, $\beta(z)$ and $b\sigma_8(z)$ assuming that dark energy perturbations are unimportant

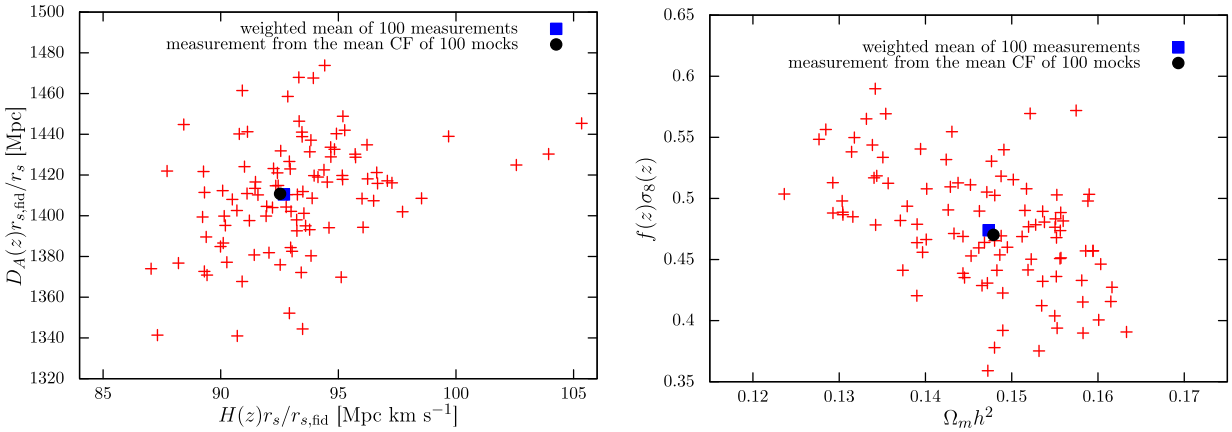

Figure 3. Left panel: The small red crosses indicate the measurements of $\frac{H(z)r_{\rm s}}{r_{\rm s,fid}}$ and $\frac{D_{\rm A}(z)r_{\rm s,fid}}{r_{\rm s}}$ from 100 individual CMASS mock catalogues. We show their weighted mean (with inverse variance weighting; blue square) and the measurement from the mean correlation function of the 100 mock catalogues (black circle); Right panel: The small red crosses indicate the measurements of $\Omega_{\rm m}\,h^2$ and $f\sigma_8$ from 100 individual CMASS mock catalogues.

(valid in the simplest dark energy models). Thus we are able to extract constraints from clustering data that are independent of dark energy.

4 RESULTS

4.1 Validate the methodology using mock catalogues

In this section, we will test our methodology by applying it to the mock catalogues. We first demonstrate that using the mean of the correlation functions is equivalent to using individual correlation functions from the mocks. We obtain the measurements from the first 100 CMASS mock catalogues within $0.43 < z < 0.75$. We use the fast model only and do not include the polynomial modelling of the systematics in these tests. The left panel of Fig. 3 shows the distribution of the measurements of $H(z_{\rm eff})r_{\rm s}/r_{\rm s,fid}$ and $D_{\rm A}(z_{\rm eff})r_{\rm s,fid}/r_{\rm s}$, where $r_{\rm s}$ is the comoving sound horizon at the drag epoch and $r_{\rm s,fid} = 147.66$ Mpc is the sound scale of the fiducial cosmology used in this study. We also show the measurements from the weighted mean (using inverse variance weighting) of 100 correlation functions from these mocks. One can see that the weighted mean of the 100 individual measurements (blue square) is very close to the measurement from the mean correlation function from 100 mocks (black circle). We conclude that one can use the mean correlation function to represent the tests for multiple correlation functions. The right panel of Fig. 3 shows the scatter of the measurements of $\Omega_{\rm m}\,h^2$ and $f\sigma_8(z)$ from the same analysis given above.

Note that the computing time is still expensive even after speeding up the analysis using the fast–slow model method described in previous sections. Therefore, instead of applying the test using the correlation function from an individual mock catalogue, we use the mean of the correlation functions from all the mocks. From these tests, we can see whether our methodology would introduce some bias or not. A small bias can be better detected using 2000 rather than 100 mock correlation functions. Therefore, we validate our methodology by applying our methodology on the mean correlation functions from 2000 mocks for different redshift bins and present the results in Table 1. One can see that for all the parameters in all the redshift bins, we recover the input parameters to within 0.3σ. We show the results using the calibrated dewiggle model in Appendix A which also recovers the input parameters within reasonable precision, 0.6σ. However, given that they are more realistic, we use the results from the Gaussian streaming model as our fiducial results.

4.2 Measurements of cosmological parameters from BOSS galaxy clustering

We now present the dark energy model independent measurements of the parameters $\{H(z), D_{\rm A}(z), \Omega_{\rm m}\,h^2, \beta(z), \text{and } b\sigma_8(z)\}$, obtained by using the method described in previous sections. We also present derived parameters including $H(z)\frac{r_{\rm s}}{r_{\rm s,fid}}$, $D_{\rm A}(z)\frac{r_{\rm s,fid}}{r_s}$, $f(z)\sigma_8(z)$ and $D_V(z)\frac{r_{\rm s,fid}}{r_s}$ with

$$D_V(z) \equiv \left[(1+z)^2 D_{\rm A}(z)^2 \frac{cz}{H(z)}\right]^{\frac{1}{3}}, \tag{21}$$

where $r_{\rm s}$ is the comoving sound horizon at the drag epoch calculated by CAMB and $r_{\rm s,fid} = 147.66$ Mpc is the $r_{\rm s}$ of the fiducial cosmology used in this study (same as the one used by the mock catalogues). We use $r_{\rm s}/r_{\rm s,fid}$ instead of $r_{\rm s}$ since it is more insensitive to the approximate formula used for computing $r_{\rm s}$. $D_V(z)$ is the effective distance which can be measured from the spherical averaged correlation function or power spectrum (e.g. see Eisenstein et al. 2005).

Table 2 lists the mean and standard deviation obtained from the MCMC likelihood analysis from the DR12 galaxy correlation function. We measure $\{D_{\rm A}(z)r_{\rm s,fid}/r_{\rm s}$, $H(z)r_{\rm s}/r_{\rm s,fid}$, $f(z)\sigma_8(z)$, $\Omega_{\rm m}\,h^2\}$, $D_V r_{\rm s}^{\rm fid}/r_{\rm s}$, β, $b\sigma_8$ (they are not independent), using the range $40\,h^{-1}$ Mpc $< s < 180\,h^{-1}$ Mpc, at the different redshift bins, i.e. $0.15 < z < 0.43$, $0.43 < z < 0.75$, $0.15 < z < 0.30$, $0.30 < z < 0.43$, $0.43 < z < 0.55$, $0.55 < z < 0.75$. The effective redshifts are $\{0.32, 0.59, 0.24, 0.37, 0.49, 0.64\}$. The covariance matrices for these measurements can be found in the Appendix.

To conveniently compare with other measurements using CMASS sample within $0.43 < z < 0.7$ (we are using $0.43 < z < 0.75$), we extrapolated our measurements at $z = 0.57$: $H(0.57)r_{\rm s}/r_{\rm s,fid} = 95.5 \pm 2.7\,{\rm km\,s^{-1}\,Mpc^{-1}}$, $D_{\rm A}(0.57)r_{\rm s,fid}/r_{\rm s} = 1404 \pm 23$ Mpc, and $D_V(0.57)r_{\rm s,fid}/r_{\rm s} = 2050 \pm 22$ Mpc (see table 9 of Alam et al. 2017).

In the next section, we will describe how to use our results of single-probe measurements combining with other data set to constrain the parameters of given dark energy models.

Table 1. Measurements of $\Omega_{\rm m}h^2$, $f(z)\sigma_8(z)$, $\frac{H(z)r_{\rm s}}{r_{\rm s,fid}}$, $\frac{D_{\rm A}(z)r_{\rm s,fid}}{r_{\rm s}}$ and $\frac{D_V(z)r_{\rm s,fid}}{r_{\rm s}}$ from the mean of 2000 correlation functions, where the unit of $H(z)$ is km s^{-1} Mpc^{-1} and the units of $D_{\rm A}(z)$ and $D_V(z)$ are Mpc. The effective redshifts are $\{0.32, 0.59, 0.24, 0.37, 0.49, 0.64\}$. We show the means and standard deviations, input values, the differences between mean and input values (in percentage), and the standard deviations in percentage.

	$\Omega_{\rm m}h^2$	$f\sigma_8(z)$	$\frac{H(z)r_{\rm s}}{r_{\rm s,fid}}$	$\frac{D_{\rm A}(z)r_{\rm s,fid}}{r_{\rm s}}$	$\frac{D_V(z)r_{\rm s,fid}}{r_{\rm s}}$
$0.15 < z < 0.43$	0.143 ± 0.016	0.465 ± 0.085	80.6 ± 4.7	989 ± 31	1267 ± 29
Input values	0.14105	0.481	80.16	990.2	1269.19
Deviation & uncertainty (per cent)	1.2 & 11.5	−3.3 & 17.6	0.5 & 5.8	−0.1 & 3.2	−0.2 & 2.3
$0.43 < z < 0.75$	0.139 ± 0.013	0.478 ± 0.061	94.2 ± 3.4	1416 ± 25	2119 ± 30
Input values	0.14105	0.4786	94.09	1409.26	2113.37
Deviation & uncertainty (per cent)	−1.2 & 9.0	−0.2 & 12.8	0.1 & 3.7	0.5 & 1.7	0.3 & 1.4
$0.15 < z < 0.30$	0.139 ± 0.016	0.460 ± 0.105	80.0 ± 10.7	792 ± 69	957 ± 76
Input values	0.14105	0.4751	76.63	807.25	979.874
Deviation & uncertainty (per cent)	−1.5 & 11.3	−3.3 & 22.1	4.4 & 14.0	−1.9 & 8.6	−2.3 & 7.8
$0.30 < z < 0.43$	0.142 ± 0.015	0.493 ± 0.111	83.6 ± 7.9	1090 ± 49	1438 ± 57
Input values	0.14105	0.4829	82.52	1088.59	1440.62
Deviation & uncertainty (per cent)	1.0 & 10.9	2.1 & 22.9	1.3 & 9.5	0.2 & 4.5	−0.2 & 4.0
$0.43 < z < 0.55$	0.140 ± 0.016	0.478 ± 0.084	88.1 ± 4.9	1286 ± 39	1830 ± 41
Input values	0.14105	0.4827	88.59	1283.41	1823.53
Deviation & uncertainty (per cent)	−0.7 & 11.3	−1.0 & 17.4	−0.5 & 5.6	0.2 & 3.1	0.4 & 2.3
$0.55 < z < 0.75$	0.136 ± 0.015	0.490 ± 0.078	98.5 ± 5.8	1462 ± 42	2238 ± 43
Input values	0.14105	0.4754	96.97	1461.99	2248.92
Deviation & uncertainty (per cent)	−0.7 & 10.4	1.7 & 16.4	1.6 & 6.0	0.0 & 2.9	−0.5 & 1.9

Table 2. Our measurements of $\{D_{\rm A}(z)r_{\rm s,fid}/r_{\rm s}, H(z)r_{\rm s}/r_{\rm s,fid}, f(z)\sigma_8(z), \Omega_{\rm m}h^2\}$, $D_Vr_{\rm s,fid}/r_{\rm s}$, β, $b\sigma_8$, from BOSS DR12 data at the different redshift bins stated, using the range $40\,h^{-1}$ Mpc $< s < 180\,h^{-1}$ Mpc; $r_{\rm s,fid}$ is 147.66 Mpc in this study; the unit of $H(z)$ is km s^{-1} Mpc^{-1} and the units of $D_{\rm A}(z)$ and $D_V(z)$ are Mpc. The effective redshifts of these redshift bins are $\{0.32, 0.59, 0.24, 0.37, 0.49, 0.64\}$.

	$0.15 < z < 0.43$	$0.43 < z < 0.75$	$0.15 < z < 0.30$	$0.30 < z < 0.43$	$0.43 < z < 0.55$	$0.55 < z < 0.75$
$D_{\rm A}r_{\rm s}^{\rm fid}/r_{\rm s}$	956 ± 28	1421 ± 23	826 ± 45	993 ± 65	1288 ± 31	1444 ± 41
$Hr_{\rm s}/r_{\rm s}^{\rm fid}$	75.0 ± 4.0	96.7 ± 2.7	78.8 ± 5.6	74.8 ± 6.3	87.5 ± 4.8	98.4 ± 3.7
$f\sigma_8$	0.397 ± 0.073	0.497 ± 0.058	0.493 ± 0.105	0.378 ± 0.076	0.456 ± 0.068	0.454 ± 0.064
$\Omega_{\rm m}h^2$	0.143 ± 0.017	0.137 ± 0.015	0.136 ± 0.017	0.147 ± 0.014	0.144 ± 0.016	0.140 ± 0.017
$D_Vr_{\rm s}^{\rm fid}/r_{\rm s}$	1268 ± 26	2106 ± 23	987 ± 40	1402 ± 69	1837 ± 36	2220 ± 39
β	0.301 ± 0.066	0.435 ± 0.070	0.389 ± 0.096	0.287 ± 0.067	0.367 ± 0.072	0.410 ± 0.077
$b\sigma_8$	1.332 ± 0.099	1.154 ± 0.090	1.287 ± 0.129	1.332 ± 0.137	1.256 ± 0.112	1.120 ± 0.094

5 CONSTRAINING COSMOLOGICAL PARAMETERS OF GIVEN DARK ENERGY MODELS

5.1 Likelihood derivation

In this section, we describe the steps to combine our results with other data sets assuming some dark energy models. Here, we use the results from two redshift bins, $0.15 < z < 0.43$ (LOWZ) and $0.43 < z < 0.75$ (CMASS), as an example. For a given model and cosmological parameters, one can compute $H(z)\frac{r_{\rm s}}{r_{\rm s,fid}}$, $D_{\rm A}(z)\frac{r_{\rm s,fid}}{r_s}$, $f(z)\sigma_8(z)$ and $\Omega_{\rm m}h^2$. From Tables B1 and B2 in Appendix B and the standard deviations in Table 2, one can compute the covariance matrices, $M_{ij,\,\rm CMASS}$ and $M_{ij,\,\rm LOWZ}$, of these four parameters. Then, $\chi^2_{\rm CMASS}$ and $\chi^2_{\rm LOWZ}$ can be computed by

$$\chi^2_{\rm CMASS} = \Delta_{\rm CMASS} M^{-1}_{ij,\rm CMASS} \Delta_{\rm CMASS}, \tag{22}$$

and

$$\chi^2_{\rm LOWZ} = \Delta_{\rm LOWZ} M^{-1}_{ij,\rm LOWZ} \Delta_{\rm LOWZ}, \tag{23}$$

where

$$\Delta_{\rm CMASS} = \begin{pmatrix} D_{\rm A}(z)\frac{r_{\rm s,fid}}{r_s} - 1421 \\ H(z)\frac{r_{\rm s}}{r_{\rm s,fid}} - 96.7 \\ f(z)\sigma_8(z) - 0.497 \\ \Omega_{\rm m}h^2 - 0.137 \end{pmatrix}, \tag{24}$$

$$\Delta_{\rm LOWZ} = \begin{pmatrix} D_{\rm A}(z)\frac{r_{\rm s,fid}}{r_s} - 956 \\ H(z)\frac{r_{\rm s}}{r_{\rm s,fid}} - 75.0 \\ f(z)\sigma_8(z) - 0.397 \\ \Omega_{\rm m}h^2 - 0.143 \end{pmatrix}, \tag{25}$$

$$M_{ij,\rm CMASS} = \begin{pmatrix} 0.53559E+03 & 0.27875E+02 & 0.70092E+00 & -0.29507E-01 \\ 0.27875E+02 & 0.74866E+01 & 0.85855E-01 & -0.92898E-02 \\ 0.70092E+00 & 0.85855E-01 & 0.33643E-02 & -0.51341E-03 \\ -0.29507E-01 & -0.92898E-02 & -0.51341E-03 & 0.22673E-03 \end{pmatrix},$$

Table 3. The cosmological constraints from two redshift bins and four redshift bins combined with Planck data assuming ΛCDM, non-flat ΛCDM (oΛCDM), wCDM, w_0w_aCDM and ow_0w_aCDM. The units of H_0 are km s^{-1} Mpc^{-1}.

	Ω_m	H_0	σ_8	Ω_k	w or w_0	w_a
Planck+2bins (ΛCDM)	0.307 ± 0.008	67.9 ± 0.6	0.815 ± 0.009	0	-1	0
Planck+4bins (ΛCDM)	0.306 ± 0.009	67.9 ± 0.7	0.815 ± 0.009	0	-1	0
Planck+2bins (oΛCDM)	0.307 ± 0.008	67.8 ± 0.8	0.815 ± 0.009	0.000 ± 0.003	-1	0
Planck+4bins (oΛCDM)	0.306 ± 0.010	68.0 ± 1.0	0.815 ± 0.010	0.000 ± 0.003	-1	0
Planck+2bins (wCDM)	0.304 ± 0.013	68.3 ± 1.5	0.819 ± 0.015	0	-1.02 ± 0.06	0
Planck+4bins (wCDM)	0.304 ± 0.016	68.3 ± 1.7	0.818 ± 0.017	0	-1.01 ± 0.06	0
Planck+2bins (owCDM)	0.305 ± 0.015	68.2 ± 1.5	0.819 ± 0.017	0.000 ± 0.003	-1.02 ± 0.08	0
Planck+4bins (owCDM)	0.304 ± 0.017	68.2 ± 1.8	0.817 ± 0.017	0.000 ± 0.004	-1.02 ± 0.08	0
Planck+2bins (w_0w_aCDM)	0.310 ± 0.021	67.8 ± 2.2	0.815 ± 0.019	0	-0.95 ± 0.22	-0.22 ± 0.63
Planck+4bins (w_0w_aCDM)	0.314 ± 0.021	67.2 ± 2.2	0.810 ± 0.019	0	-0.86 ± 0.22	-0.50 ± 0.67
Planck+2bins (ow_0w_aCDM)	0.312 ± 0.020	67.4 ± 2.2	0.813 ± 0.018	-0.002 ± 0.004	-0.90 ± 0.23	-0.49 ± 0.75
Planck+4bins (ow_0w_aCDM)	0.316 ± 0.022	66.9 ± 2.3	0.809 ± 0.019	-0.002 ± 0.004	-0.82 ± 0.22	-0.73 ± 0.73

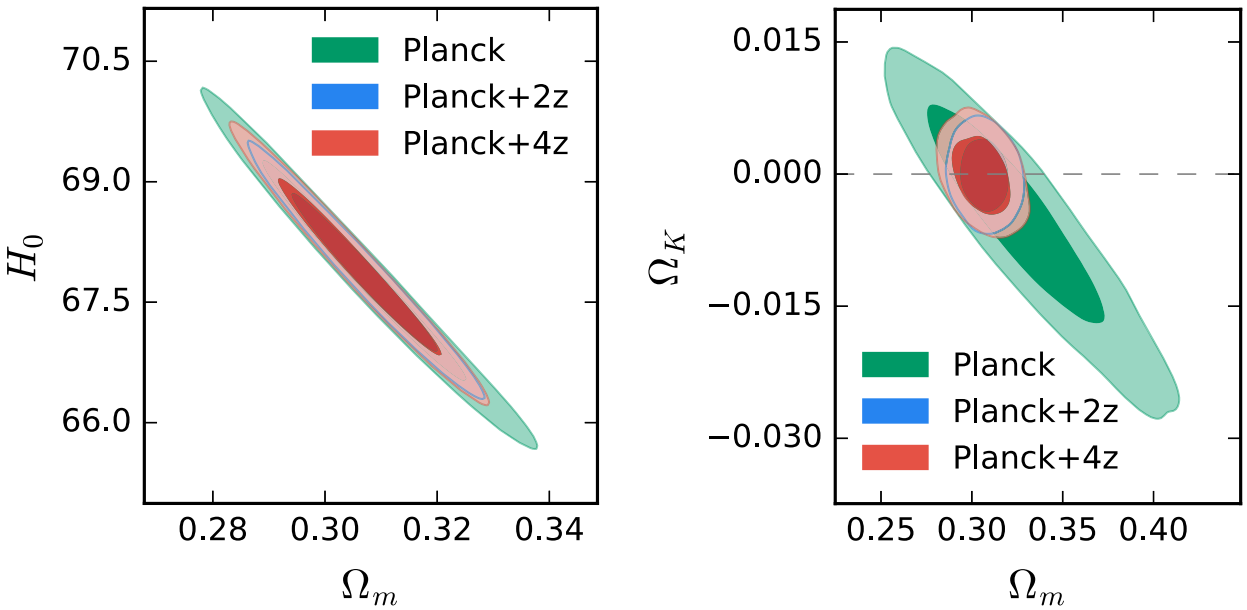

Figure 4. Left panel: 2D marginalized contours for 68 per cent and 95 per cent confidence levels for Ω_m and H_0 (ΛCDM model assumed) from *Planck*-only (green), *Planck*+CMASS (one bin)+LOWZ (one bin) (blue), and *Planck*+CMASS (two bins)+LOWZ (two bins) (red); right panel: 2D marginalized contours for 68 per cent and 95 per cent confidence level for Ω_m and Ω_k (oΛCDM model assumed). One can see that Ω_k is consistent with 0 which corresponds to the flat universe.

and

$$M_{ij,\mathrm{LOWZ}} = \begin{pmatrix} 0.77636E+03 & 0.43792E+02 & 0.11413E+01 & 0.86090E-01 \\ 0.43792E+02 & 0.16253E+02 & 0.19856E+00 & 0.21477E-01 \\ 0.11413E+01 & 0.19856E+00 & 0.53875E-02 & 0.69008E-04 \\ 0.86090E-01 & 0.21477E-01 & 0.69008E-04 & 0.29001E-03 \end{pmatrix}.$$

One can include the cosmological constraints from the SDSS/BOSS galaxy clustering by adding $\chi^2_{\mathrm{LOWZ}} + \chi^2_{\mathrm{CMASS}}$ in the MCMC analysis, due to the negligible correlation of these samples.

5.2 Constraining dark energy parameters combining with external data sets

In this section, we present examples of combining our galaxy clustering results with the *Planck* CMB data assuming specific dark energy models. The *Planck* data set we use is the *Planck* 2015 measurements (Adam et al. 2016; Ade et al. 2016a). The reference likelihood code (Planck Collaboration XI 2016) was downloaded from the Planck Legacy Archive.[5] Here we combine the *Plik* baseline likelihood for high multipoles ($30 \leq \ell \leq 2500$) using the TT, TE and EE power spectra, and the *Planck* low-ℓ multipole likelihood in the range $2 \leq \ell \leq 29$ (hereafter lowTEB). We also include the *Planck* 2015 lensing likelihood (Ade et al. 2016b), constructed from the measurements of the power spectrum of the lensing potential (hereafter referred as 'lensing'). When using the *Planck* lensing likelihood, the A_{lens} parameter is always set to 1 (Ade et al. 2016a).

Table 3 shows the cosmological constraints assuming flat ΛCDM, oΛCDM (non-flat ΛCDM), wCDM (constant equation of state of dark energy), owCDM (non-flat wCDM), w_0w_aCDM (time-dependent equation of state) and ow_0w_aCDM (non-flat w_0w_aCDM). In addition to using two redshift bins, we use four redshift bins but we do not find any improvement in terms of constraining

[5] PLA: http://pla.esac.esa.int/

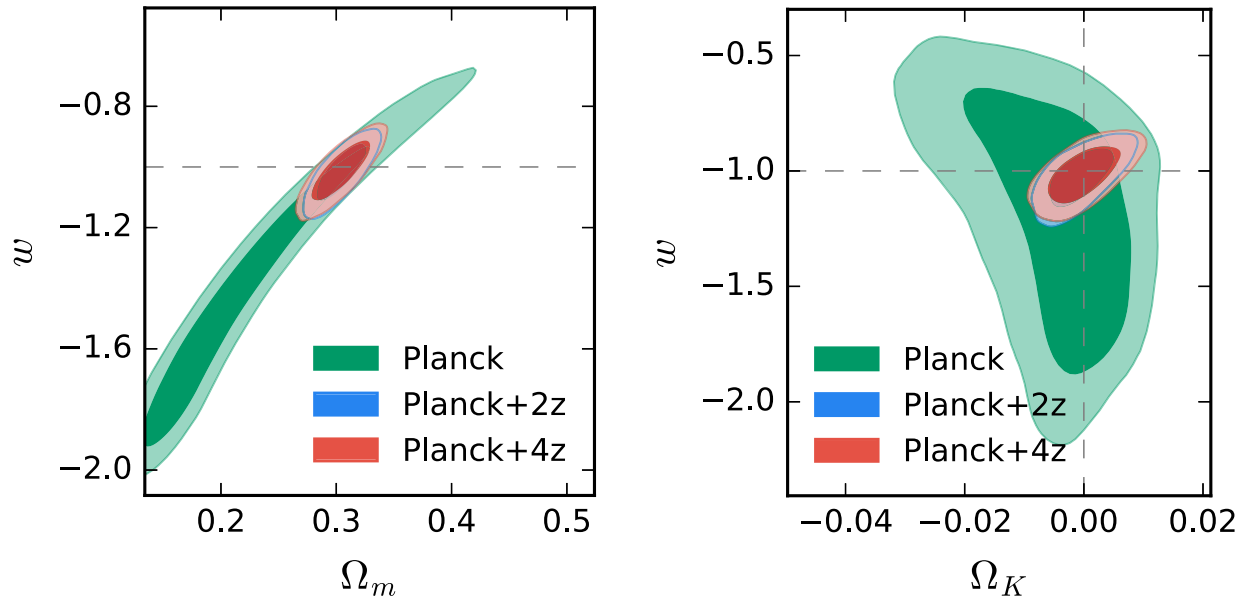

Figure 5. Left panel: 2D marginalized contours for 68 per cent and 95 per cent confidence level for Ω_m and w (wCDM model assumed) from *Planck*-only (green), *Planck*+CMASS (one bin)+LOWZ (one bin) (blue), and *Planck*+CMASS (two bins)+LOWZ (two bins) (red); right panel: 2D marginalized contours for 68 per cent and 95 per cent confidence level for Ω_k and w (owCDM model assumed). One can see that Ω_k is consistent with 0 and w is consistent with -1 which corresponds to the ΛCDM.

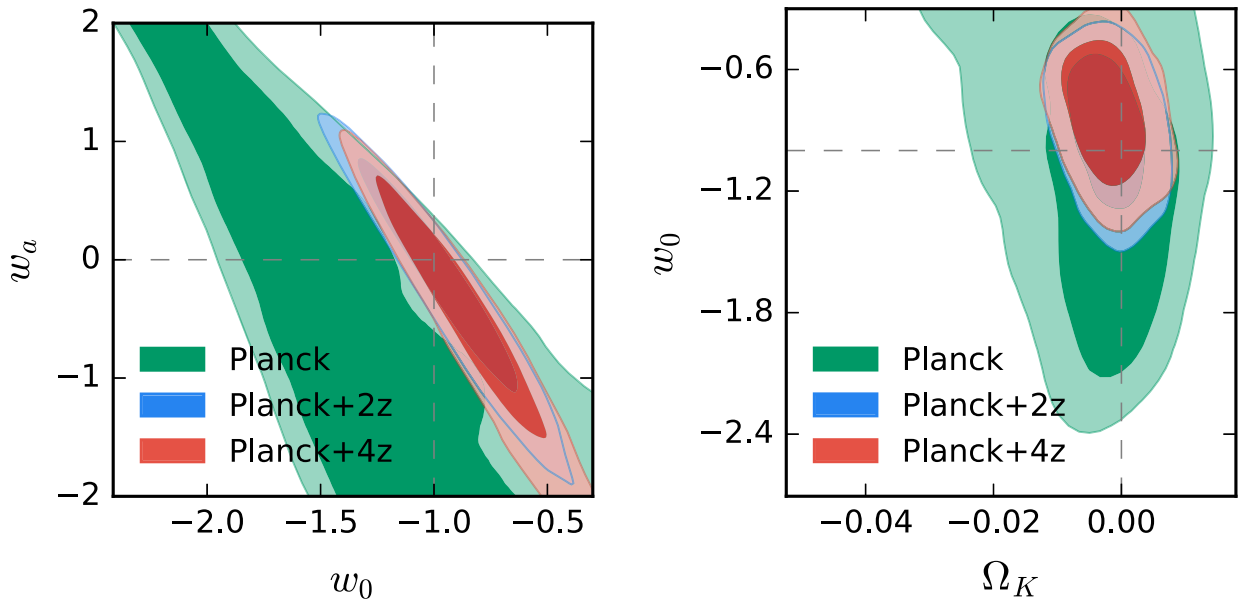

Figure 6. Left panel: 2D marginalized contours for 68 per cent and 95 per cent confidence level for w_0 and w_a (w_0w_aCDM model assumed) from *Planck*-only (green), *Planck*+CMASS (one bin)+LOWZ (one bin) (blue), and *Planck*+CMASS (two bins)+LOWZ (two bins) (red); right panel: 2D marginalized contours for 68 per cent and 95 per cent confidence level for Ω_k and w_0 (ow_0w_aCDM model assumed). One can see that w_0 and w_a are consistent with -1 and 0, respectively, which correspond to the ΛCDM.

cosmological parameters. It should indicate that the models we are testing are still simple and do not benefit from higher redshift sensitivity. In addition, some information (pair counts) would be lost when we slice the sample into more bins. In Figs 4–6, we show 2D marginalized contours for 68 per cent and 95 per cent confidence levels for Ω_m and H_0 (ΛCDM model assumed); Ω_m and Ω_k (oΛCDM model assumed); Ω_m and w (wCDM model assumed); Ω_k and w (owCDM model assumed); w_0 and w_a (w_0w_aCDM model assumed); Ω_k and w_0 (ow_0w_aCDM model assumed). One can see that all the constraints are consistent with flat ΛCDM.

6 COMPARISON WITH OTHER WORKS

We compile the measurements of $f(z)\sigma_8(z)$, $D_A(z)/r_s$, $H(z)^*r_s$ and $D_V(z)/r_s$ from various galaxy surveys in Tables C1–C3 in Appendix C. We have included the measurements from VIMOS-VLT Deep Survey (VVDS; Guzzo et al. 2008), 2dFGRS (Percival et al. 2004), Six-degree-Field Galaxy Survey (6dFGS; Beutler et al. 2011, 2012), WiggleZ (Blake et al. 2011a,b, 2012; Contreras et al. 2013), SDSS-II/DR7 (Percival et al. 2010; Chuang et al. 2012; Chuang & Wang 2012, 2013a,b; Padmanabhan et al. 2012;

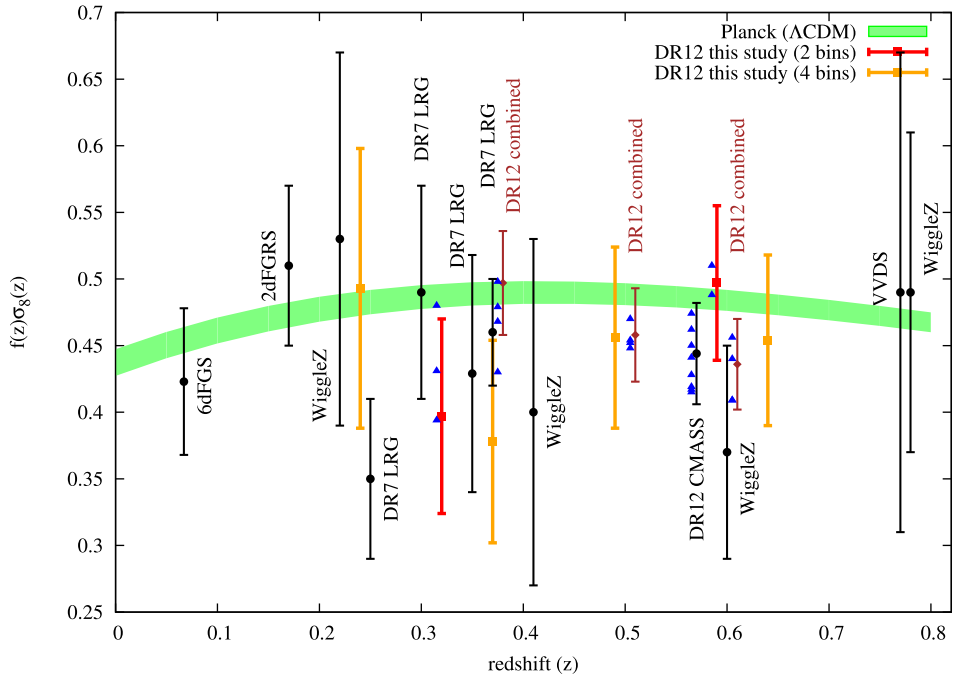

Figure 7. We compare the constraints of $f(z)\sigma_8(z)$ from CMB data (*Planck*) with our measurements (red squares), other measurements from SDSS galaxy sample and the measurements compiled by Samushia et al. (2013) (black circles). We also compare with the consensus measurements from Alam et al. (2017) (BOSS collaboration paper for final data release; brown diamond points). The constraints from CMB are obtained assuming a ΛCDM model.

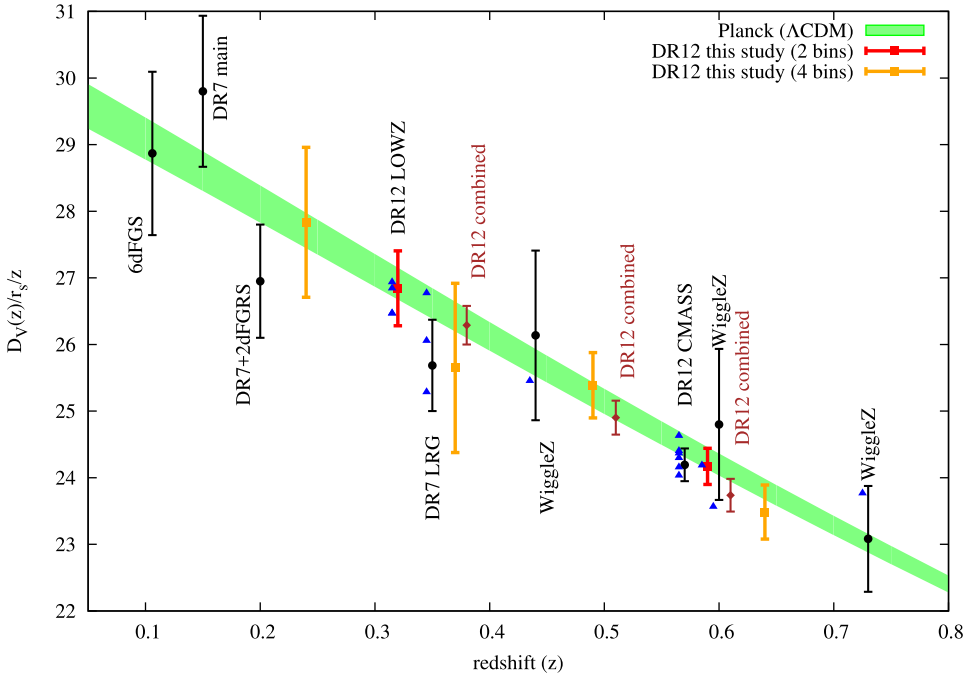

Figure 8. We compare the constraints of $\frac{D_V(z)}{r_s z}$ from CMB data (*Planck*) with our measurements (red squares), and other measurements [black circles and blue triangles; Percival et al. 2010; Beutler et al. 2011; Blake et al. 2011a; Chuang et al. 2012; Chuang & Wang 2012; Padmanabhan et al. 2012; Anderson et al. 2013, 2014a; Beutler et al. 2014; Samushia et al. 2014; Tojeiro et al. 2014; Ross et al. 2015; Alam et al. 2017 (BOSS collaboration paper for final data release)]. The consensus values from Alam et al. (2017) are shown with brown diamond points. When there are more than one measurements at the same redshift, we mark one of the measurements using a black circle with error bar (i.e. the measurement from Chuang & Wang 2012 at $z = 0.35$ and the consensus values from Cuesta et al. 2016 at $z = 0.57$) and mark the others with blue triangles with a slight shift in redshift to make the plot more clear. The constraints from CMB are obtained assuming a ΛCDM model.

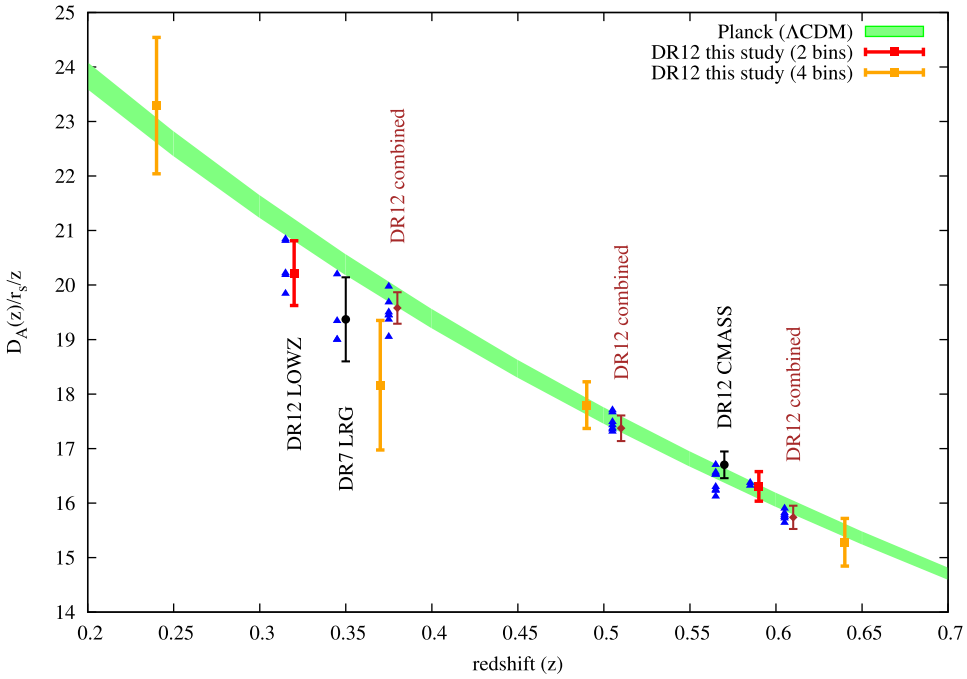

Figure 9. We compare the constraints of $\frac{D_A(z)}{r_s z}$ from CMB data (*Planck*) with our measurements (red squares), and other measurements [black circles and blue triangles; Chuang & Wang 2012, 2013a,b; Chuang et al. 2013; Kazin et al. 2013; Xu et al. 2013; Anderson et al. 2014a,b; Beutler et al. 2014; Hemantha et al. 2014; Wang 2014; Cuesta et al. 2016; Gil-Marín et al. 2016a,b, Alam et al. (2017) (BOSS collaboration paper for final data release) and its companion papers including this paper and Ross et al. (2017); Vargas-Magaña et al. (2016); Beutler et al. (2017a,b); Grieb et al. (2017); Pellejero-Ibanez et al. (2017); Sanchez et al. (2017b); Satpathy et al. (2017)]. The consensus values from Alam et al. (2017) are shown with brown diamond points. When there are more than one measurements at the same redshift, we mark one of the measurements using a black circle with error bar (i.e. the measurement from Chuang & Wang 2012 at $z = 0.35$ and the consensus values from Cuesta et al. 2016 at $z = 0.57$) and mark the others with blue triangles with a slight shift in redshift to make the plot more clear. The constraints from CMB are obtained assuming a ΛCDM model.

Samushia et al. 2012; Seo et al. 2012; Xu et al. 2013; Hemantha, Wang & Chuang 2014; Ross et al. 2015) SDSS-III/BOSS (Reid et al. 2012; Anderson et al. 2013, 2014a,b; Chuang et al. 2013; Kazin et al. 2013; Beutler et al. 2014; Reid et al. 2014; Sanchez et al. 2014; Samushia et al. 2014; Tojeiro et al. 2014; Wang 2014; Alam et al. 2015a; Cuesta et al. 2016; Gil-Marín et al. 2016a,b), Alam et al. (2017) (BOSS collaboration paper for final data release) and its companion papers including this paper and Vargas-Magaña et al. (2016); Beutler et al. (2017a,b); Grieb et al. (2017); Pellejero-Ibanez et al. (2017; Ross et al. (2017); Sanchez et al. (2017b); Satpathy et al. (2017)).

To be able to include more measurements, we quote $D_V(z)/r_s$ instead of $D_V(z)r_{s,fid}/r_s$ since $r_{s,fid}$ was not provided in some references. In Figs 7–10, we compare the constraints of $f(z)\sigma_8(z)$, $D_V(z)/r_s$, $D_A(z)/r_s$ and $H(z)r_s$ from CMB data (*Planck* assuming ΛCDM) with the measurements from galaxy clustering analyses compiled in Tables C1–C3.

In these figures, when there are many measurements that correspond to the same redshift, we show the mean and error bar for only one of them (as indicated in the caption) and show only the mean values indicated with triangles for the rest of the measurements. We also slightly shift the redshift to make the figures more clear. Since we are using the CMASS galaxy sample with an extended redshift range ($0.43 < z < 0.75$) compared to other studies using the CMASS galaxy sample ($0.43 < z < 0.7$), the comparison cannot be done directly. However, our measurements agree very well with the prediction from *Planck* data assuming ΛCDM, and so do the measurements from previous works. One can see that the measurements of $D_V(z)/r_s$ from different analyses but at the same redshift agree with each other. However, the measurements of $H(z)r_s/r_{s,fid}$ and $D_A(z)r_{s,fid}/r_s$ have larger scatter. This is expected since $D_V(z)/r_s$ is driven by the BAO feature in the monopole. But, $H(z)r_s$ and $D_A(z)/r_s$ are correlated with the shape of BAO feature which has larger uncertainties among different models.

There seems to be a slight deviation between our $f(z)\sigma_8(z)$ measurements and *Planck* ΛCDM prediction, e.g. in our measurement at $z = 0.32$ (Fig. 7). In fact, the measurements are consistent with *Planck* result within 1σ if one looks at the two-dimensional contours of $f(z)\sigma_8(z)$ and $\Omega_m h^2$ shown in Fig. 11. One can see that there is some correlation between $f(z)\sigma_8(z)$ and $\Omega_m h^2$.

7 SUMMARY

We present measurements of the anisotropic galaxy clustering from the CMASS and LOWZ samples of the final date release (DR12) of the SDSS-III BOSS and obtain constraints on the Hubble expansion rate $H(z)$, the angular-diameter distance $D_A(z)$, the normalized growth rate $f(z)\sigma_8(z)$, and the physical matter density $\Omega_m h^2$. We analyse the broad-range shape of quasi-linear scales of the monopole and quadrupole correlation functions to obtain cosmological constraints at different redshift bins. In addition to the two redshift bins, i.e. LOWZ ($z_{LOWZ} = 0.32$) and CMASS ($z_{CMASS} = 0.59$), we split each galaxy sample into two bins (for a total of four redshift bins) and obtain the measurements at $z = \{0.24, 0.37, 0.49, 0.64\}$ to increase the sensitivity of redshift evolution. However, we do not find improvement in terms of constraining different dark energy model parameters. It might indicate that the dark energy component is stable in the redshift range considered.

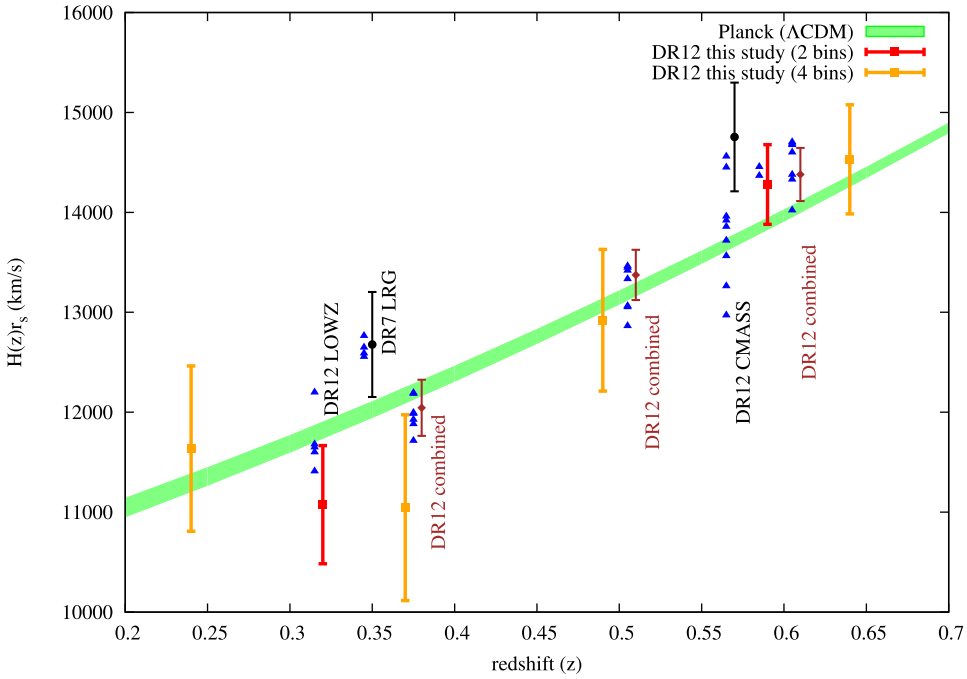

Figure 10. We compare the constraints of $H(z)r_s$ (km s^{-1}) from CMB data (*Planck*) with our measurements (red squares), and other measurements [black circles and blue triangles; Chuang & Wang 2012, 2013a,b; Chuang et al. 2013; Kazin et al. 2013; Xu et al. 2013; Anderson et al. 2014a,b; Beutler et al. 2014; Hemantha et al. 2014; Wang 2014; Gil-Marín et al. 2016a,b; Cuesta et al. 2016, Alam et al. 2017 (BOSS collaboration paper for final data release) and its companion papers including this paper and Vargas-Magaña et al. (2016); Beutler et al. (2017a,b); Grieb et al. (2017); Pellejero-Ibanez et al. (2017); Ross et al. (2017); Sanchez et al. (2017b); Satpathy et al. (2017)]. The consensus values from Alam et al. (2017) are shown with brown diamond points. When there are more than one measurements at the same redshift, we mark one of the measurements using a black circle with error bar (i.e. the measurement from Chuang & Wang 2012 at $z = 0.35$ and the consensus values from Cuesta et al. 2016 at $z = 0.57$) and mark the others with blue triangles with a slight shift in redshift to make the plot more clear. The constraints from CMB are obtained assuming a ΛCDM model.

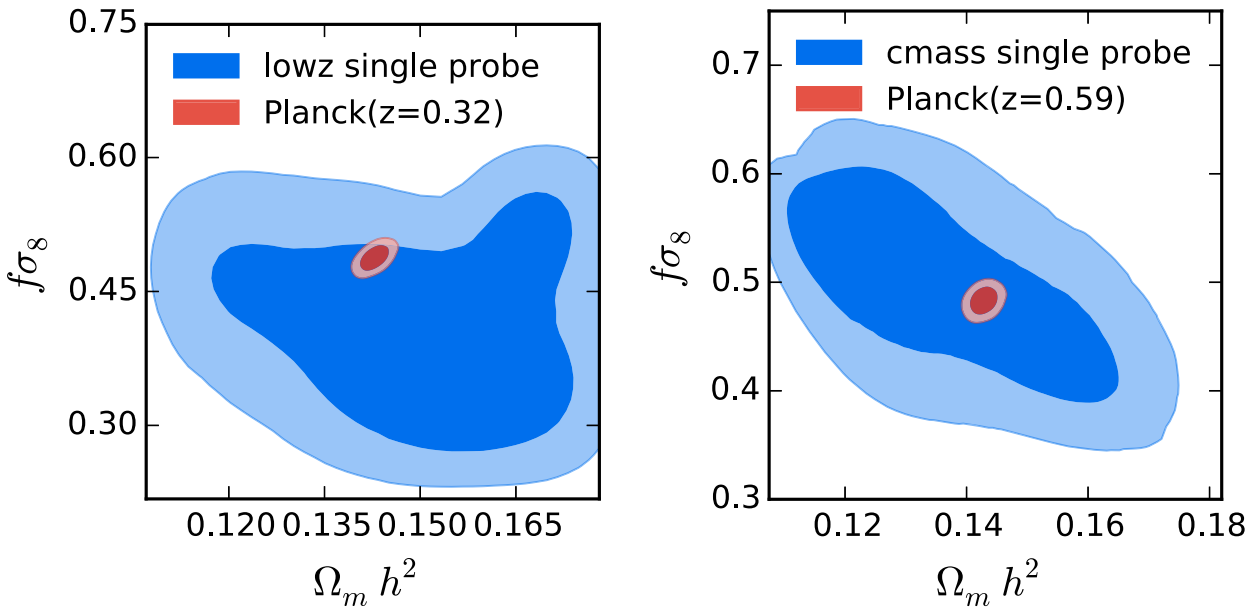

Figure 11. 2D marginalized contours for 68 per cent and 95 per cent confidence level for the measurement of $f(z)\sigma_8(z)$ and $\Omega_m h^2$ from the LOWZ sample comparing with the *Planck* prediction at the same redshift (left panel for $z = 0.32$ and right panel for $z = 0.59$; assuming ΛCDM).

We adopt wide and flat priors on all model parameters in order to ensure the results are those of a 'single-probe' galaxy clustering analysis. We also marginalize over three nuisance terms that account for potential observational systematics affecting the measured monopole. The Monte Carlo Markov Chain analysis with such wide priors and additional polynomial functions is computationally expensive for advanced theoretical models. We have developed and validated a new methodology to speed this up by scanning the parameter space using a fast model first and then applying importance sampling using a slower but more accurate model.

Our measurements for DR12 galaxy sample, using the range $40\,h^{-1}$ Mpc $< s < 180\,h^{-1}$ Mpc, are $\{D_A(z)r_{s,fid}/r_s,\ H(z)r_s/r_{s,fid},\ f(z)\sigma_8(z),\ \Omega_m h^2\} = \{956 \pm 28$ Mpc, $75.0 \pm 4.0\,km\,s^{-1}\,Mpc^{-1},\ 0.397 \pm 0.073,\ 0.143 \pm 0.017\}$ at $z = 0.32$ and $\{1421 \pm 23$ Mpc, $96.7 \pm 2.7\,km\,s^{-1}\,Mpc^{-1},\ 0.497 \pm 0.058,\ 0.137 \pm 0.015\}$ at $z = 0.59$ where r_s is the comoving sound horizon at the drag epoch and $r_{s,fid} = 147.66$ Mpc is the sound scale of the fiducial cosmology used in this study. Combining our measurements with *Planck* data, we obtain $\Omega_m = 0.306 \pm 0.009$, $H_0 = 67.9 \pm 0.7\,km\,s^{-1}\,Mpc^{-1}$, and $\sigma_8 = 0.815 \pm 0.009$ assuming ΛCDM; $\Omega_k = 0.000 \pm 0.003$ assuming oCDM; $w = -1.01 \pm 0.06$ assuming wCDM; and $w_0 = -0.95 \pm 0.22$ and $w_a = -0.22 \pm 0.63$ assuming w_0w_aCDM. The results show no tension with the flat ΛCDM cosmological paradigm.

ACKNOWLEDGEMENTS

CC and FP acknowledge support from the Spanish MICINN's Consolider-Ingenio 2010 Programme under grant MultiDark CSD2009-00064 and AYA2010-21231-C02-01 grant. CC was also supported by the Comunidad de Madrid under grant HEPHACOS S2009/ESP-1473. CC was supported as a MultiDark fellow. MPI acknowledges support from MINECO under the grant AYA2012-39702-C02-01. GR is supported by the National Research Foundation of Korea (NRF) through NRF-SGER 2014055950 funded by the Korean Ministry of Education, Science and Technology (MoEST), and by the faculty research fund of Sejong University in 2016. MVM acknowledges support from Programa de Apoyo a Proyectos de Investigación e Innovación Tecnológica (PAPITT) No IA102516, Proyecto Conacyt Fronteras No 281 and Proyecto LANCAD-UNAM-DGTIC-319.

We acknowledge the use of the CURIE supercomputer at Très Grand Centre de calcul du CEA in France through the French participation into the PRACE research infrastructure, the SuperMUC supercomputer at Leibniz Supercomputing Centre of the Bavarian Academy of Science in Germany, the TEIDE-HPC (High Performance Computing) supercomputer in Spain, and the Hydra cluster at Instituto de Física Teórica, (UAM/CSIC) in Spain.

Funding for SDSS-III has been provided by the Alfred P. Sloan Foundation, the Participating Institutions, the National Science Foundation and the U.S. Department of Energy Office of Science. The SDSS-III web site is http://www.sdss3.org/.

SDSS-III is managed by the Astrophysical Research Consortium for the Participating Institutions of the SDSS-III Collaboration including the University of Arizona, the Brazilian Participation Group, Brookhaven National Laboratory, Carnegie Mellon University, University of Florida, the French Participation Group, the German Participation Group, Harvard University, the Instituto de Astrofisica de Canarias, the Michigan State/Notre Dame/JINA Participation Group, Johns Hopkins University, Lawrence Berkeley National Laboratory, Max Planck Institute for Astrophysics, Max Planck Institute for Extraterrestrial Physics, New Mexico State University, New York University, Ohio State University, Pennsylvania State University, University of Portsmouth, Princeton University, the Spanish Participation Group, University of Tokyo, University of Utah, Vanderbilt University, University of Virginia, University of Washington and Yale University.

REFERENCES

Abazajian K. et al., 2005, AJ, 129, 1755
Abazajian K. N. et al., 2009, ApJS, 182
Adam R. et al., 2016, A&A, 594, A1
Ade P. A. R. et al., 2014a, A&A, 571, A1
Ade P. A. R. et al., 2014b, A&A, 571, A16
Ade P. A. R. et al., 2016a, A&A, 594, A13
Ade P. A. R. et al., 2016b, A&A, 594, A15
Aihara H. et al., 2011, ApJS, 193, 29
Alam S., Ho S., Vargas-Magaña M., Schneider D. P., 2015a, MNRAS, 453, 1754
Alam S. et al., 2015b, ApJS, 219, 12
Alam S. et al., 2017, MNRAS, 470, 2617
Alcock C., Paczynski B., 1979, Nature, 281, 358
Anderson L. et al., 2013, MNRAS, 427, 3435
Anderson L. et al., 2014a, MNRAS, 441, 24
Anderson L. et al., 2014b, MNRAS, 439, 83
Bennett C. L. et al., 2013, ApJS, 208, 20
Beutler F. et al., 2011, MNRAS, 416, 3017
Beutler F. et al., 2012, MNRAS, 423, 3430
Beutler F. et al., 2014, MNRAS, 443, 1065
Beutler F. et al., 2017a, MNRAS, 466, 2242
Beutler F. et al., 2017b, MNRAS, 464, 3409
Bianchi D., Chiesa M., Guzzo L., 2015, MNRAS, 446, 75
Blake C. et al., 2011a, MNRAS, 418, 1707
Blake C. et al., 2011b, MNRAS, 415, 2876
Blake C. et al., 2012, MNRAS, 425, 405
Bolton A. S. et al., 2012, AJ, 144, 144
Carlson J., Reid B., White M., 2013, MNRAS, 429, 1674
Chuang C.-H., Wang Y., 2012, MNRAS, 426, 226
Chuang C.-H., Wang Y., 2013a, MNRAS, 435, 255
Chuang C.-H., Wang Y., 2013b, MNRAS, 431, 2634
Chuang C.-H., Wang Y., Hemantha M. D. P., 2012, MNRAS, 423, 1474
Chuang C.-H. et al., 2013, MNRAS, 433, 3559
Chuang C.-H. et al., 2015, MNRAS, 452, 686
Chuang C.-H. et al., 2016, MNRAS, 461, 3781
Colless M. et al., 2001, MNRAS, 328, 1039
Colless M. et al., 2003, preprint (astro-ph/0306581)
Contreras C. et al., 2013, MNRAS, 430, 924
Crocce M., Scoccimarro R., 2006, Phys. Rev. D., 73, 063520
Cuesta A. J. et al., 2016, MNRAS, 457, 1770
Dawson K. S. et al., 2013, AJ, 145, 10
Drinkwater M. J. et al., 2010, MNRAS, 401, 1429
Eisenstein D. J., Hu W., 1998, ApJ, 496, 605
Eisenstein D. J. et al., 2005, ApJ, 633, 560
Eisenstein D. J., Seo H.-j., White M. J., 2007, ApJ, 664, 660
Eisenstein D. J. et al., 2011, AJ, 142, 72
Feldman H. A., Kaiser N., Peacock J. A., 1994, ApJ, 426, 23
Fukugita M., Ichikawa T., Gunn J. E., Doi M., Shimasaku K., Schneider D. P., 1996, AJ, 111, 1748
Gil-Marín H. et al., 2016a, MNRAS, 460, 4210
Gil-Marín H. et al., 2016b, MNRAS, 460, 4188
Green J. et al., 2012, preprint (arXiv:1208.4012)
Grieb J. N. et al., 2017, MNRAS, 467, 2085
Gunn J. E. et al., 1998, AJ, 116, 3040
Gunn J. E. et al., 2006, AJ, 131, 2332
Guzzo L. et al., 2008, Nature, 451, 541
Hartlap J., Simon P., Schneider P., 2007, A&A, 464, 399
Hemantha M. D. P., Wang Y., Chuang C.-H., 2014, MNRAS, 445, 3737
Kaiser N., 1987, MNRAS, 227, 1
Kazin E. A. et al., 2013, MNRAS, 435, 64
Kazin E. A. et al., 2014, MNRAS, 441, 3524
Kitaura F.-S., Yepes G., Prada F., 2014, MNRAS, 439, 21
Kitaura F.-S., Gil-Marín H., Scoccola C., Chuang C.-H., Müller V., Yepes G., Prada F., 2015, MNRAS, 450, 1836
Kitaura F.-S. et al., 2016a, Phys. Rev. Lett., 116, 171301
Kitaura F.-S. et al., 2016b, MNRAS, 456, 4156
Landy S. D., Szalay A. S., 1993, ApJ, 412, 64
Laureijs R. et al., 2011, preprint (arXiv:1110.3193)
Lewis A., Bridle S., 2002, Phys. Rev. D, 66, 103511
Lewis A., Challinor A., Lasenby A., 2000, ApJ, 538, 473

Liang Y., Zhao C., Chuang C.-H., Kitaura F.-S., Tao C., 2016, MNRAS, 459, 4020
Matsubara T., 2008, Phys. Rev. D., 77, 063530
Oka A., Saito S., Nishimichi T., Taruya A., Yamamoto K., 2014, MNRAS, 439, 2515
Okumura T., Hand N., Seljak U., Vlah Z., Desjacques V., 2015, Phys. Rev. D., 92, 103516
Padmanabhan N., Xu X., Eisenstein D. J., Scalzo R., Cuesta A. J., Mehta K. T., Kazin E., 2012, MNRAS, 427, 2132
Parkinson D. et al., 2012, Phys. Rev. D., 86, 103518
Pellejero-Ibanez M. et al., 2017, MNRAS, 468, 4116
Percival W. J., White M., 2009, MNRAS, 393, 297
Percival W. J. et al., 2004, MNRAS, 353, 1201
Percival W. J. et al., 2010, MNRAS, 401, 2148
Perlmutter S. et al., 1999, ApJ, 517, 565
Planck Collaboration XI, 2016, A&A, 594, A11
Press W. H., Teukolsky S. A., Vetterling W. T., Flannery B. P., 2007, Numerical Recipes in C. The Art of Scientific Computing. University Press, Cambridge
Reid B. A., White M., 2011, MNRAS, 417, 1913
Reid B. A. et al., 2012, MNRAS, 426, 2719
Reid B. A., Seo H.-J., Leauthaud A., Tinker J. L., White M., 2014, MNRAS, 444, 476
Reid B. et al., 2016, MNRAS, 455, 1553
Riess A. G. et al., 1998, AJ, 116, 1009
Rodríguez-Torres S. A. et al., 2016, MNRAS, 460, 1173
Ross A. J. et al., 2012, MNRAS, 424, 564
Ross A. J., Samushia L., Howlett C., Percival W. J., Burden A., Manera M., 2015, MNRAS, 449, 835
Ross A. J. et al., 2017, MNRAS, 464, 1168
Salazar-Albornoz S. et al., 2017, MNRAS, 468, 2938
Samushia L., Percival W. J., Raccanelli A., 2012, MNRAS, 420, 2102
Samushia L. et al., 2013, MNRAS, 429, 1514
Samushia L. et al., 2014, MNRAS, 439, 3504
Sanchez A. G. et al., 2014, MNRAS, 440, 2692
Sanchez A. G. et al., 2017a, MNRAS, 464, 1493
Sanchez A. G. et al., 2017b, MNRAS, 464, 1640
Satpathy S. et al., 2017, MNRAS, 469, 1369
Schlegel D. et al., 2011, preprint (arXiv:1106.1706)
Seo H.-J. et al., 2012, ApJ, 761, 13
Slepian Z. et al., 2016, preprint (arXiv:1607.06098)
Slepian Z. et al., 2017a, MNRAS, 468, 1070
Slepian Z. et al., 2017b, MNRAS, 469, 1738
Smee S. et al., 2013, AJ, 146, 32
Song Y.-S., Percival W. J., 2009, J. Cosmol. Astropart. Phys., 0910, 004
Taruya A., Nishimichi T., Bernardeau F., 2013, Phys. Rev. D., 87, 083509
Taruya A., Nishimichi T., Bernardeau F., Hiramatsu T., Koyama K., 2014, Phys. Rev. D., 90, 123515
Tojeiro R. et al., 2014, MNRAS, 440, 2222
Van Waerbeke L., Mellier Y., 2003, in Gravitational Lensing: A Unique Tool for Cosmology Aussois, Savoie, France, January 5–11, 2003 Gravitational Lensing by Large Scale Structures: A Review. preprint (astro-ph/0305089).
Vargas-Magaña M. et al., 2016, preprint (arXiv:1610.03506)
Verde L. et al., 2002, MNRAS, 335, 432
Vlah Z., Seljak U., Okumura T., Desjacques V., 2013, J. Cosmol. Astropart. Phys., 1310, 053
Vlah Z., White M., Aviles A., 2015, J. Cosmol. Astropart. Phys., 1509, 014
Wang Y., 2008, J. Cosmol. Astropart. Phys., 0805, 021
Wang Y., 2012, MNRAS, 423, 3631
Wang Y., 2014, MNRAS, 443, 2950
Wang L., Reid B., White M., 2014, MNRAS, 437, 588
Wang Y. et al., 2017, MNRAS, 469, 3762
White M., 2014, MNRAS, 439, 3630
Xu X., Cuesta A. J., Padmanabhan N., Eisenstein D. J., McBride C. K., 2013, MNRAS, 431, 2834
York D. G. et al., 2000, AJ, 120, 1579
Zhao G.-B. et al., 2017, MNRAS, 466, 762

APPENDIX A: PERFORMANCE OF CALIBRATED DEWIGGLE MODEL

We present the results using the calibrated dewiggle model in Table A1 which also recovers the input parameters with reasonable precision (0.6σ). It shows that our methodology does not bias significantly our results.

Table A1. Measurements from the mean of 2000 correlation functions using dewiggle model, where the unit of $H(z)$ is km s^{-1} Mpc^{-1} and the units of $D_A(z)$ and $D_V(z)$ are Mpc.

	$\Omega_m h^2$	$f\sigma_8(z)$	$\frac{H(z)r_s}{r_{s,fid}}$	$\frac{D_A(z)r_{s,fid}}{r_s}$	$\frac{D_V(z)r_{s,fid}}{r_s}$
$0.15 < z < 0.43$	0.150 ± 0.015	0.464 ± 0.086	79.9 ± 5.2	991 ± 33	1272 ± 30
Input values	0.14105	0.481	80.16	990.2	1269.19
Deviation & uncertainty (per cent)	6.3 & 10.6	−3.6 & 18.0	−0.4 & 6.5	0.0 & 3.3	0.2 & 2.3
$0.43 < z < 0.75$	0.150 ± 0.014	0.490 ± 0.055	93.6 ± 3.5	1416 ± 27	2124 ± 30
Input values	0.14105	0.4786	94.09	1409.26	2113.37
Deviation & uncertainty (per cent)	6.2 & 9.8	2.3 & 11.5	−0.5 & 3.7	0.5 & 1.9	0.5 & 1.4
$0.15 < z < 0.30$	0.143 ± 0.016	0.469 ± 0.111	77.6 ± 8.8	802 ± 58	973 ± 56
Input values	0.14105	0.4751	76.63	807.25	979.874
Deviation & uncertainty (per cent)	1.7 & 11.6	−1.3 & 23.3	1.2 & 11.4	−0.7 & 7.2	−0.7 & 5.7
$0.30 < z < 0.43$	0.147 ± 0.016	0.489 ± 0.099	82.4 ± 7.1	1090 ± 45	1444 ± 46
Input values	0.14105	0.4829	82.52	1088.59	1440.62
Deviation & uncertainty (per cent)	3.9 & 11.2	1.3 & 20.6	−0.1 & 8.6	0.1 & 4.2	0.2 & 3.2
$0.43 < z < 0.55$	0.147 ± 0.016	0.494 ± 0.077	88.0 ± 5.6	1287 ± 37	1832 ± 43
Input values	0.14105	0.4827	88.59	1283.41	1823.53
Deviation & uncertainty (per cent)	4.1 & 11.0	2.3 & 15.9	−0.6 & 6.4	0.3 & 2.9	0.5 & 2.3
$0.55 < z < 0.75$	0.145 ± 0.015	0.495 ± 0.071	97.0 ± 5.1	1468 ± 37	2255 ± 44
Input values	0.14105	0.4754	96.97	1461.99	2248.92
Deviation & uncertainty (per cent)	3.0 & 10.5	4.1 & 14.9	0.0 & 5.3	0.4 & 2.5	0.3 & 1.9

APPENDIX B: MEASURED COVARIANCE MATRIX

We show the normalized covariance matrices (also called correlation matrices) of our measurements in Table B1 to B6. A normalized covariance matrix is defined by

$$N_{ij} = \frac{C_{ij}}{\sqrt{C_{ii}C_{jj}}}, \tag{B1}$$

where C_{ij} is the covariance matrix.

Table B1. Normalized covariance matrix of the measurements from DR12 galaxy sample of $0.15 < z < 0.43$. The units of $D_{\rm A}(z)$ and $D_V(z)$ are Mpc.

	$D_{\rm A}(z)\frac{r_{\rm s,fid}}{r_{\rm s}}$	$H(z)\frac{r_{\rm s}}{r_{\rm s,fid}}$	$f\sigma_8(z)$	$\Omega_{\rm m}h^2$	$D_V(z)\frac{r_{\rm s,fid}}{r_{\rm s}}$	$\beta(z)$	$b\sigma_8(z)$
$D_{\rm A}(z)\frac{r_{\rm s,fid}}{r_{\rm s}}$	1.0000	0.3899	0.5581	0.1814	0.6045	0.4718	0.0160
$H(z)\frac{r_{\rm s}}{r_{\rm s,fid}}$	0.3899	1.0000	0.6710	0.3128	−0.4973	0.6559	−0.2362
$f\sigma_8(z)$	0.5581	0.6710	1.0000	0.0552	−0.0562	0.9476	−0.2714
$\Omega_{\rm m}h^2$	0.1814	0.3128	0.0552	1.0000	−0.1057	0.0364	0.0756
$D_V(z)\frac{r_{\rm s,fid}}{r_{\rm s}}$	0.6045	−0.4973	−0.0562	−0.1057	1.0000	−0.1237	0.2183
$\beta(z)$	0.4718	0.6559	0.9476	0.0364	−0.1237	1.0000	−0.5544
$b\sigma_8(z)$	0.0160	−0.2362	−0.2714	0.0756	0.2183	−0.5544	1.0000

Table B2. Normalized covariance matrix of the measurements from DR12 galaxy sample of $0.43 < z < 0.75$. The units of $D_{\rm A}(z)$ and $D_V(z)$ are Mpc.

	$D_{\rm A}(z)\frac{r_{\rm s,fid}}{r_{\rm s}}$	$H(z)\frac{r_{\rm s}}{r_{\rm s,fid}}$	$f\sigma_8(z)$	$\Omega_{\rm m}h^2$	$D_V(z)\frac{r_{\rm s,fid}}{r_{\rm s}}$	$\beta(z)$	$b\sigma_8(z)$
$D_{\rm A}(z)\frac{r_{\rm s,fid}}{r_{\rm s}}$	1.0000	0.4402	0.5222	−0.0847	0.6206	0.4513	−0.1722
$H(z)\frac{r_{\rm s}}{r_{\rm s,fid}}$	0.4402	1.0000	0.5410	−0.2255	−0.4306	0.4293	−0.0799
$f\sigma_8(z)$	0.5222	0.5410	1.0000	−0.5879	0.0509	0.8951	−0.3739
$\Omega_{\rm m}h^2$	−0.0847	−0.2255	−0.5879	1.0000	0.1152	−0.5034	0.1335
$D_V(z)\frac{r_{\rm s,fid}}{r_{\rm s}}$	0.6206	−0.4306	0.0509	0.1152	1.0000	0.0769	−0.1022
$\beta(z)$	0.4513	0.4293	0.8951	−0.5034	0.0769	1.0000	−0.7402
$b\sigma_8(z)$	−0.1722	−0.0799	−0.3739	0.1335	−0.1022	−0.7402	1.0000

Table B3. Normalized covariance matrix of the measurements from DR12 galaxy sample of $0.15 < z < 0.30$. The units of $D_{\rm A}(z)$ and $D_V(z)$ are Mpc.

	$D_{\rm A}(z)\frac{r_{\rm s,fid}}{r_{\rm s}}$	$H(z)\frac{r_{\rm s}}{r_{\rm s,fid}}$	$f\sigma_8(z)$	$\Omega_{\rm m}h^2$	$D_V(z)\frac{r_{\rm s,fid}}{r_{\rm s}}$	$\beta(z)$	$b\sigma_8(z)$
$D_{\rm A}(z)\frac{r_{\rm s,fid}}{r_{\rm s}}$	1.0000	0.1492	0.5334	0.0738	0.8167	0.3523	0.2295
$H(z)\frac{r_{\rm s}}{r_{\rm s,fid}}$	0.1492	1.0000	0.4036	0.1066	−0.4465	0.4294	−0.2197
$f\sigma_8(z)$	0.5334	0.4036	1.0000	−0.1680	0.2417	0.9096	−0.1677
$\Omega_{\rm m}h^2$	0.0738	0.1066	−0.1680	1.0000	0.0131	−0.1872	0.0796
$D_V(z)\frac{r_{\rm s,fid}}{r_{\rm s}}$	0.8167	−0.4465	0.2417	0.0131	1.0000	0.0625	0.3418
$\beta(z)$	0.3523	0.4294	0.9096	−0.1872	0.0625	1.0000	−0.5489
$b\sigma_8(z)$	0.2295	−0.2197	−0.1677	0.0796	0.3418	−0.5489	1.0000

Table B4. Normalized covariance matrix of the measurements from DR12 galaxy sample of $0.30 < z < 0.43$. The units of $D_{\rm A}(z)$ and $D_V(z)$ are Mpc.

	$D_{\rm A}(z)\frac{r_{\rm s,fid}}{r_{\rm s}}$	$H(z)\frac{r_{\rm s}}{r_{\rm s,fid}}$	$f\sigma_8(z)$	$\Omega_{\rm m}h^2$	$D_V(z)\frac{r_{\rm s,fid}}{r_{\rm s}}$	$\beta(z)$	$b\sigma_8(z)$
$D_{\rm A}(z)\frac{r_{\rm s,fid}}{r_{\rm s}}$	1.0000	0.1042	0.5015	0.1169	0.8364	0.1788	0.5662
$H(z)\frac{r_{\rm s}}{r_{\rm s,fid}}$	0.1042	1.0000	0.4615	−0.1769	−0.4533	0.5100	−0.1488
$f\sigma_8(z)$	0.5015	0.4615	1.0000	−0.2777	0.1991	0.8736	0.0567
$\Omega_{\rm m}h^2$	0.1169	−0.1769	−0.2777	1.0000	0.2003	−0.2214	−0.0643
$D_V(z)\frac{r_{\rm s,fid}}{r_{\rm s}}$	0.8364	−0.4533	0.1991	0.2003	1.0000	−0.1108	0.5839
$\beta(z)$	0.1788	0.5100	0.8736	−0.2214	−0.1108	1.0000	−0.4223
$b\sigma_8(z)$	0.5662	−0.1488	0.0567	−0.0643	0.5839	−0.4223	1.0000

Table B5. Normalized covariance matrix of the measurements from DR12 galaxy sample of $0.43 < z < 0.55$. The units of $D_A(z)$ and $D_V(z)$ are Mpc.

	$D_A(z)\frac{r_{s,fid}}{r_s}$	$H(z)\frac{r_s}{r_{s,fid}}$	$f\sigma_8(z)$	$\Omega_m h^2$	$D_V(z)\frac{r_{s,fid}}{r_s}$	$\beta(z)$	$b\sigma_8(z)$
$D_A(z)\frac{r_{s,fid}}{r_s}$	1.0000	0.3189	0.4258	0.0776	0.5088	0.2947	0.0573
$H(z)\frac{r_s}{r_{s,fid}}$	0.3189	1.0000	0.5740	0.0618	−0.6525	0.5351	−0.2326
$f\sigma_8(z)$	0.4258	0.5740	1.0000	−0.2981	−0.1848	0.9001	−0.3283
$\Omega_m h^2$	0.0776	0.0618	−0.2981	1.0000	0.0109	−0.1441	−0.1903
$D_V(z)\frac{r_{s,fid}}{r_s}$	0.5088	−0.6525	−0.1848	0.0109	1.0000	−0.2533	0.2576
$\beta(z)$	0.2947	0.5351	0.9001	−0.1441	−0.2533	1.0000	−0.6958
$b\sigma_8(z)$	0.0573	−0.2326	−0.3283	−0.1903	0.2576	−0.6958	1.0000

Table B6. Normalized covariance matrix of the measurements from DR12 galaxy sample of $0.55 < z < 0.75$. The units of $D_A(z)$ and $D_V(z)$ are Mpc.

	$D_A(z)\frac{r_{s,fid}}{r_s}$	$H(z)\frac{r_s}{r_{s,fid}}$	$f\sigma_8(z)$	$\Omega_m h^2$	$D_V(z)\frac{r_{s,fid}}{r_s}$	$\beta(z)$	$b\sigma_8(z)$
$D_A(z)\frac{r_{s,fid}}{r_s}$	1.0000	0.4299	0.4490	0.0544	0.7736	0.3330	0.0055
$H(z)\frac{r_s}{r_{s,fid}}$	0.4299	1.0000	0.4408	−0.0347	−0.2390	0.3523	−0.0624
$f\sigma_8(z)$	0.4490	0.4408	1.0000	−0.4533	0.1753	0.8950	−0.3339
$\Omega_m h^2$	0.0544	−0.0347	−0.4533	1.0000	0.0815	−0.3508	0.0318
$D_V(z)\frac{r_{s,fid}}{r_s}$	0.7736	−0.2390	0.1753	0.0815	1.0000	0.1114	0.0513
$\beta(z)$	0.3330	0.3523	0.8950	−0.3508	0.1114	1.0000	−0.7106
$b\sigma_8(z)$	0.0055	−0.0624	−0.3339	0.0318	0.0513	−0.7106	1.0000

APPENDIX C: COMPILATIONS OF MEASUREMENTS FROM OTHER WORKS AND THIS STUDY

We compile the measurements of $f(z)\sigma_8(z)$, $D_A(z)/r_s$, $H(z)^\star r_s$ and $D_V(z)/r_s$ from various galaxy surveys in Table C1, C2 and C3. We have included the measurements from VIMOS-VLT Deep Survey (VVDS; Guzzo et al. 2008), 2dFGRS (Percival et al. 2004), Six-degree-Field Galaxy Survey (6dFGS; Beutler et al. 2011, 2012), WiggleZ (Blake et al. 2011a,b, 2012; Contreras et al. 2013), SDSS-II/DR7 (Percival et al. 2010; Chuang et al. 2012; Chuang & Wang 2012, 2013a,b; Padmanabhan et al. 2012; Samushia et al. 2012; Seo et al. 2012; Xu et al. 2013; Hemantha et al. 2014; Ross et al. 2015) SDSS-III/BOSS (Reid et al. 2012; Anderson et al. 2013, 2014b; Chuang et al. 2013; Kazin et al. 2013; Anderson et al. 2014a; Beutler et al. 2014; Reid et al. 2014; Samushia et al. 2014; Sanchez et al. 2014; Tojeiro et al. 2014; Wang 2014; Alam et al. 2015a; Cuesta et al. 2016; Gil-Marín et al. 2016a,b), Pellejero-Ibanez et al. (2016); Vargas-Magaña et al. (2016), Alam et al. (2017) (BOSS collaboration paper for final data release) and its companion papers including this paper and Beutler et al. (2017a); Beutler et al. (2017b); Grieb et al. (2017); Ross et al. (2017); Sanchez et al. (2017b); Satpathy et al. (2017). To be able to include more measurements, we quote $D_V(z)/r_s$ instead of $D_V(z)r_{s,fid}/r_s$ since $r_{s,fid}$ was not provided in some references.

Table C1. Measurements of $f(z)\sigma_8(z)$ from different galaxy surveys, including SDSS-II (DR7), SDSS-III (DR9, DR11, DR12), 6dFGS, WiggleZ, 2dFGRS and VVDS.

Redshift	$f(z)\sigma_8(z)$	Data	Reference
0.64	0.454 ± 0.064	DR12	This study
0.59	0.497 ± 0.058	DR12	
0.49	0.456 ± 0.068	DR12	
0.37	0.378 ± 0.076	DR12	
0.32	0.397 ± 0.073	DR12	
0.24	0.493 ± 0.105	DR12	
0.59	0.51 ± 0.047	DR12	Pellejero-Ibanez et al. (2016)
0.32	0.431 ± 0.063	DR12	
0.61	0.436 ± 0.034	DR12	Alam et al. (2017)
0.51	0.458 ± 0.035	DR12	(BOSS consensus results)
0.38	0.497 ± 0.039	DR12	
0.61	0.456 ± 0.052	DR12	Satpathy et al. (2017)
0.51	0.452 ± 0.058	DR12	
0.38	0.43 ± 0.054	DR12	
0.61	0.409 ± 0.044	DR12	Beutler et al. (2017a)
0.51	0.454 ± 0.051	DR12	
0.38	0.479 ± 0.054	DR12	
0.61	0.409 ± 0.041	DR12	Grieb et al. (2017)
0.51	0.448 ± 0.038	DR12	
0.38	0.498 ± 0.045	DR12	
0.61	0.44 ± 0.039	DR12	Sanchez et al. (2017b)
0.51	0.47 ± 0.042	DR12	
0.38	0.468 ± 0.053	DR12	
0.59	0.488 ± 0.06	DR12	Chuang et al. (2016)
0.57	0.444 ± 0.038	DR12	Gil-Marín et al. (2016b)
0.32	0.394 ± 0.062	DR12	
0.57	0.417 ± 0.045	DR11	Sanchez et al. (2014)
0.32	0.48 ± 0.10	DR11	
0.57	0.441 ± 0.044	DR11	Samushia et al. (2014)
0.57	0.419 ± 0.044	DR11	Beutler et al. (2014)
0.57	0.462 ± 0.041	DR11	Alam et al. (2015a)
0.57	0.45 ± 0.011	DR10	Reid et al. (2014)
0.57	0.428 ± 0.069	DR9	Chuang et al. (2013)
0.57	0.415 ± 0.034	DR9	Reid et al. (2012)
0.57	0.474 ± 0.075	DR9	Wang (2014)
0.3	0.49 ± 0.08	DR7	Oka et al. (2014)
0.37	0.46 ± 0.04	DR7	Samushia et al. (2012)
0.25	0.35 ± 0.06	DR7	
0.35	0.429 ± 0.089	DR7	Chuang & Wang (2013a)
0.067	0.423 ± 0.055	6dFGS	Beutler et al. (2012)
0.44	0.413 ± 0.08	WiggleZ	Blake et al. (2012)
0.6	0.39 ± 0.063	WiggleZ	
0.73	0.437 ± 0.072	WiggleZ	
0.22	0.42 ± 0.07	WiggleZ	Blake et al. (2011b)
0.41	0.45 ± 0.04	WiggleZ	
0.6	0.43 ± 0.04	WiggleZ	
0.78	0.38 ± 0.04	WiggleZ	
0.17	0.51 ± 0.06	2dFGRS	Percival et al. (2004)
0.77	0.49 ± 0.18	VVDS	Guzzo et al. (2008)

Table C2. Measurements of $D_V(z)/r_s$ from different galaxy surveys, including SDSS-II (DR7), SDSS-III (DR9, DR11, DR12), 2dFGRS, 6dFGS and WiggleZ. To be able to include more measurements, we use $D_V(z)/r_s$ instead of $D_V(z)r_{s,fid}/r_s$ since $r_{s,fid}$ (Mpc) was not provided in some literatures. In addition, we have included an approximation $r_{s,EH}/r_{s,CAMB} = 1.027$ to correct the different ways of estimating the sound horizon in different analyses.

Redshift	$D_V(z)/r_s$	$r_{s,fid}$	Data	Reference
0.64	15.03 ± 0.26	147.66	DR12	This study
0.59	14.26 ± 0.16	147.66	DR12	
0.49	12.44 ± 0.24	147.66	DR12	
0.37	9.49 ± 0.47	147.66	DR12	
0.32	8.59 ± 0.18	147.66	DR12	
0.24	6.68 ± 0.27	147.66	DR12	
0.61	14.48 ± 0.15	147.78	DR12	Alam et al. (2017)
0.51	12.70 ± 0.13	147.78	DR12	(BOSS consensus results)
0.38	9.99 ± 0.11	147.78	DR12	
0.59	14.27 ± 0.18	147.66	DR12	Chuang et al. (2016)
0.57	13.79 ± 0.14	147.1	DR12	Cuesta et al. (2016)
0.32	8.59 ± 0.15	147.1	DR12	
0.57	13.70 ± 0.12		DR12	Gil-Marín et al. (2016a)
0.32	8.62 ± 0.15		DR12	
0.57	13.85 ± 0.17		DR11	Samushia et al. (2014)
0.57	13.89 ± 0.18	147.36	DR11	Beutler et al. (2014)
0.57	13.77 ± 0.13	149.28	DR11	Anderson et al. (2014a)
0.32	8.47 ± 0.17	149.28	DR11	
0.32	8.47 ± 0.17	149.28	DR11	Tojeiro et al. (2014)
0.57	14.04 ± 0.23	149.16	DR9	Anderson et al. (2013)
0.57	13.91 ± 0.30		DR9	Chuang et al. (2013)
0.35	9.12 ± 0.17		DR7	Padmanabhan et al. (2012)
0.35	8.85 ± 0.26		DR7	Chuang & Wang (2012)
0.35	8.99 ± 0.24		DR7	Chuang et al. (2012)
0.35	9.37 ± 0.31		DR7+2dFGRS	Percival et al. (2010)
0.2	5.39 ± 0.17		DR7+2dFGRS	
0.15	4.47 ± 0.17	148.69	DR7	Ross et al. (2015)
0.106	3.06 ± 0.13		6dFGS	Beutler et al. (2011)
0.44	11.50 ± 0.56	149.28	WiggleZ	Kazin et al. (2014)
0.6	14.88 ± 0.68	149.28	WiggleZ	
0.73	16.85 ± 0.58	149.28	WiggleZ	
0.44	11.20 ± 0.87		WiggleZ	Blake et al. (2011a)
0.6	14.14 ± 0.67		WiggleZ	
0.73	17.35 ± 0.93		WiggleZ	

Table C3. Measurements of $H(z)r_s$ (km s^{-1}) and $D_A(z)/r_s$ from different galaxy surveys, including SDSS-II (DR7) and SDSS-III (DR9,DR11,DR12). To be able to include more measurements, we use $D_A(z)/r_s$ and $H(z)r_s$ instead of $D_A(z)r_{s,fid}/r_s$ and $H(z)r_s/r_{s,fid}$ since $r_{s,fid}$ (Mpc) was not provided in some literatures. In addition, we have included an approximation $r_{s,EH}/r_{s,CAMB} = 1.027$ to correct the different ways of estimating the sound horizon in different analyses.

Redshift	$H(z)r_s$	$D_A(z)/r_s$	$r_{s,fid}$	Data	Reference
0.64	14530 ± 546	9.78 ± 0.28	147.66	DR12	This study
0.59	14279 ± 399	9.62 ± 0.16	147.66	DR12	
0.49	12920 ± 709	8.72 ± 0.21	147.66	DR12	
0.37	11045 ± 930	6.72 ± 0.44	147.66	DR12	
0.32	11075 ± 591	6.47 ± 0.19	147.66	DR12	
0.24	11636 ± 827	5.59 ± 0.30	147.66	DR12	
0.59	14456 ± 458	9.63 ± 0.17	147.66	DR12	Pellejero-Ibanez et al. (2016)
0.32	11680 ± 487	6.47 ± 0.18	147.66	DR12	
0.61	14379 ± 266	9.60 ± 0.13	147.78	DR12	Alam et al. (2017)
0.51	13374 ± 251	8.86 ± 0.12	147.78	DR12	(BOSS consensus results)
0.38	12044 ± 281	7.44 ± 0.11	147.78	DR12	
0.61	14601 ± 340	9.70 ± 0.17	147.78	DR12	Beutler et al. (2017a)
0.51	13418 ± 325	8.86 ± 0.14	147.78	DR12	
0.38	11926 ± 355	7.39 ± 0.12	147.78	DR12	
0.61	14675 ± 369	9.63 ± 0.18	147.78	DR12	Vargas-Magaña et al. (2016)
0.51	13448 ± 310	8.85 ± 0.13	147.78	DR12	
0.38	11882 ± 355	7.39 ± 0.11	147.78	DR12	
0.61	14689 ± 325	9.65 ± 0.18	147.78	DR12	Ross et al. (2017)
0.51	13463 ± 310	8.83 ± 0.13	147.78	DR12	
0.38	11985 ± 325	7.41 ± 0.11	147.78	DR12	
0.61	14704 ± 649	9.61 ± 0.26	147.78	DR12	Satpathy et al. (2017)
0.51	13053 ± 607	8.89 ± 0.20	147.78	DR12	
0.38	11716 ± 480	7.24 ± 0.16	147.78	DR12	
0.61	14330 ± 591	9.54 ± 0.28	147.78	DR12	Beutler et al. (2017b)
0.51	13064 ± 599	9.03 ± 0.26	147.78	DR12	
0.38	12193 ± 474	7.59 ± 0.20	147.78	DR12	
0.61	14021 ± 375	9.59 ± 0.21	147.78	DR12	Grieb et al. (2017)
0.51	12863 ± 349	8.92 ± 0.16	147.78	DR12	
0.38	11995 ± 337	7.48 ± 0.12	147.78	DR12	
0.61	14378 ± 400	9.61 ± 0.18	147.78	DR12	Sanchez et al. (2017b)
0.51	13334 ± 364	9.01 ± 0.15	147.78	DR12	
0.38	12186 ± 352	7.36 ± 0.13	147.78	DR12	
0.59	14367 ± 487	9.66 ± 0.18	147.66	DR12	Chuang et al. (2016)
0.57	14754 ± 544	9.52 ± 0.14	147.1	DR12	Cuesta et al. (2016)
0.32	11650 ± 824	6.67 ± 0.14	147.1	DR12	
0.57	13920 ± 440	9.42 ± 0.15		DR12	Gil-Marín et al. (2016b)
0.32	11410 ± 560	6.35 ± 0.19		DR12	
0.57	14560 ± 370	9.42 ± 0.13		DR12	Gil-Marín et al. (2016a)
0.32	11600 ± 600	6.66 ± 0.16		DR12	
0.57	13719 ± 486	9.42 ± 0.15	147.36	DR11	Beutler et al. (2014)
0.57	13960 ± 448	9.26 ± 0.17		DR11	Sanchez et al. (2014)
0.32	12199 ± 627	6.46 ± 0.28		DR11	
0.57	14450 ± 508	9.52 ± 0.13	149.28	DR11	Anderson et al. (2014a)
0.57	13857 ± 1163	9.44 ± 0.30	149.16	DR9	Anderson et al. (2014b)
0.57	13564 ± 906	9.29 ± 0.28		DR9	Kazin et al. (2013)
0.57	13262 ± 906	9.19 ± 0.28		DR9	Chuang et al. (2013)
0.57	12970 ± 555	9.25 ± 0.24		DR9	Wang (2014)
0.35	12590 ± 526	6.65 ± 0.26		DR7	Hemantha et al. (2014)
0.35	12556 ± 1042	7.07 ± 0.26		DR7	Xu et al. (2013)
0.35	12648 ± 1227	6.77 ± 0.47		DR7	Chuang & Wang (2013a)
0.35	12765 ± 1227	6.65 ± 0.45		DR7	Chuang & Wang (2013b)
0.35	12678 ± 526	6.78 ± 0.27		DR7	Chuang & Wang (2012)

[1]*Instituto de Física Teórica, (UAM/CSIC), Universidad Autónoma de Madrid, Cantoblanco, E-28049 Madrid, Spain*
[2]*Leibniz-Institut für Astrophysik Potsdam (AIP), An der Sternwarte 16, D-14482 Potsdam, Germany*
[3]*Instituto de Astrofísica de Canarias (IAC), C/Vía Láctea, s/n, E-38200, La Laguna, Tenerife, Spain*
[4]*Departamento Astrofísica, Universidad de La Laguna (ULL), E-38206 La Laguna, Tenerife, Spain*
[5]*Campus of International Excellence UAM+CSIC, Cantoblanco, E-28049 Madrid, Spain*
[6]*Departamento de Física Teórica M8, Universidad Autonoma de Madrid (UAM), Cantoblanco, E-28049, Madrid, Spain*
[7]*Center for Cosmology and Astroparticle Physics, Department of Physics, The Ohio State University, OH 43210, USA*
[8]*Institute of Cosmology and Gravitation, University of Portsmouth, Dennis Sciama Building, Portsmouth PO1 3FX, UK*
[9]*National Astronomy Observatories, Chinese Academy of Science, Beijing, 100012, P.R.China*
[10]*Institut de Ciències del Cosmos (ICCUB), Universitat de Barcelona (IEEC-UB), Martí i Franquès 1, E-08028 Barcelona, Spain*
[11]*Instituto de Astrofísica de Andalucía (CSIC), Glorieta de la Astronomía, E-18080 Granada, Spain*
[12]*Sorbonne Universités, Institut Lagrange de Paris (ILP), 98 bis Boulevard Arago, F-75014 Paris, France*
[13]*Laboratoire de Physique Nucléaire et de Hautes Energies, Université Pierre et Marie Curie, 4 Place Jussieu, F-75005 Paris, France*
[14]*Lawrence Berkeley National Lab, 1 Cyclotron Rd, Berkeley CA 94720, USA*
[15]*Harvard–Smithsonian Center for Astrophysics, 60 Garden Street, Cambridge, MA 02138, USA*
[16]*Universitäts-Sternwarte München, Scheinerstrasse 1, D-81679, Munich, Germany*
[17]*Max-Planck-Institut für extraterrestrische Physik, Postfach 1312, Giessenbachstr., D-85741 Garching, Germany*
[18]*McWilliams Center for Cosmology, Department of Physics, Carnegie Mellon University, 5000 Forbes Ave., Pittsburgh, PA 15213, USA*
[19]*The McWilliams Center for Cosmology, Carnegie Mellon University, 5000 Forbes Ave., Pittsburgh, PA 15213, USA*
[20]*Departments of Physics and Astronomy, University of California, Berkeley, CA 94720, USA*
[21]*Department of Physics and Astronomy, Sejong University, Seoul 143-747, Korea*
[22]*Kansas State University, Manhattan, KS 66506, USA*
[23]*National Abastumani Astrophysical Observatory, Ilia State University, 2A Kazbegi Ave., GE-1060 Tbilisi, Georgia, USA*
[24]*Brookhaven National Laboratory, Upton, NY 11973, UK*
[25]*Center for Cosmology and Particle Physics, Department of Physics, New York University, 4 Washington Place, New York, NY 10003, USA*
[26]*School of Physics and Astronomy, University of St Andrews, St Andrews, KY16 9SS, UK*
[27]*Instituto de Física, Universidad Nacional Autónoma de México, Ciudad de México, Apdo. Postal 20-364, México*
[28]*Department of Physics and Astronomy, University of Utah, 115 S 1400 E, Salt Lake City, UT 84112, USA*
[29]*Department of Chemistry and Physics, King's College, 133 North River St, Wilkes Barre, PA 18711, USA*

This paper has been typeset from a TEX/LATEX file prepared by the author.